Synthesis and Characterization of Antimony Sulphide Nanoparticles and It's Doped Forms

Islamabad

A dissertation submitted to the Department of Chemistry,
Quaid-i-Azam University, Islamabad, in partial fulfillment
of the requirements for the degree of

Master of Philosophy

in

Inorganic/Analytical Chemistry

by

Iftikhar Ahmad

Department of Chemistry
Quaid-i-Azam University
Islamabad
2013

DEDICATED

TO

MY LOVING PARENTS

TABLE OF CONTENTS

ACKNOWLEDGEMENTS

Praise and gratitude to almighty **ALLAH**, The benevolent, who bestowed upon me his blessings and through the mediation of his beloved **Prophet Muhammad** (**peace be upon him**) enlightened me with abundant resoluteness and perseverance, which enabled me to accomplish this scientific assignment objectively and successfully.I am not able to find appropriate words to offer my humble thanks and pay my immense gratitude to my most respected and worthy supervisor **Prof. Dr. Syed Ahmad Tirmizi**, who showed commendable alacrity in providing proper guidance and encouragement. During my tenure in his laboratory, I have known him as a supportive, sympathetic and principle-centered person. His overly enthusiasm and integral view on research and his mission for providing "high quality work" has made a deep impression on me. I owe him tons of gratitude for having me shown this way of research. Besides of being excellent supervisor, he was as cooperative to me. I am really glad that I have come to get know **Prof. Dr. Syed Ahmad Tirmizi** in my life.

I would like to thank all honorable teachers especially **Prof. Dr. Amin Badshah**, Chairman, Department of Chemistry, and **Prof. Dr. Saqib Ali**, Head of Inorganic/Analytical Secion, Department of Chemistry, Quaid-i-Azam University, Islamabad, for providing me all necessary facilities during my research work.

I would also like to express my deep and sincere gratitude to **Dr. Syed Mujtaba Shah**, who kept an eye on the progress of my work and always was available whenever I needed his help. His wide knowledge, logical way of thinking, constant encouragement and personal guidance has provided a good basis for the present thesis.

Special thanks must goes to my **Dr. Amir Waseem** for SEM and EDX analysis.

It will be prejudice to disregard the contribution of my uncle **Dr. Zia-ur-Rehman and Dr. Afzal Shah** at each and every level in my research.

I am grateful to all my lab-fellows **Nizam Uddin, Malik Dilshad Khan, Muhammad Wajid Shah, Aziz Ahmad, Noor Uddin** and **Muhammad Siraj Uddin** for their kind cooperation and nice company during my research work.

I express my special thanks to my loving and caring **Parents**, my uncle **Saliheen Khan** and brothers for not only supporting me at home but also helping and encouraging me at work. Without their inspiration, encouragement and understanding it would have been impossible for me to finish this work.

(Iftikhar Ahmad)

ABSTRACT

Antimony sulphide and its doped forms nanoparticles were synthesized by hydrothermal method. The nanostructures of these nanoparticles were characterized by powder X-ray diffraction analysis which have shown that materials is single crystalline phase having orthorhombic crystalline system and nanosize. Red shift in the doped forms nanoparticles was confirmed by UV-Visible spectroscopy. The Infra Red spectroscopy of the prepared nanoparticles indicated these nanoparticles and its doped forms is also revealed by shifting in the peaks. Thermogravimatric analysis suggested the stability of these nanoparticles and its doped forms. Scanning Electron Microscopy showed the morphology and rough estimation of the size of these prepared nanoparticles. The EDX confirmed the elemental composition of the pure and cadmium doped antimony sulphide nanoparticles.

LIST OF TABLES

LIST OF FIGURES

Chapter – 1

INTRODUCTION

1.1 Nanomaterials

Scientists have not across the world yet defined accurate meaning of nanomaterials, but be in agreement that they are small in size which are partially characterized, measured in nanometers. An individual hair is usually 100,000 times larger than a nanometer. One nanometer is approximately equal to 100,0000 mm. Nanoparticles are present in the environment naturally from a range of products they can be formed, such as silver carbon or natural resources like silver, but nanomaterials have a dimension between 10 to 100 nanometers and at least one dimension should be in nano range. The majority nanomaterials are very minute to be seen with the naked eye and even with common lab microscopes.

Engineered nanomaterials which are made to such a small range are often referred to as materials engineered, which can get on inimitable ocular, electrical, magnetic, electrothermal and other properties. These emergent properties have latent for enormous impacts in medicine, opticals and other fields of life. For example, nanoscience can be used to destroy cancer cells and increases the efficiency of therapy because the drugs design can target precise cells and organs in the body.

Nanomaterials can also improve the properties of cloth, cement, electronics and other equipment to make them stiffer and strong and until now they were light in weight. They are very useful in electronics because of their size dimension, they can be used to bind with and neutralize toxins and they can also be used in ecological remediation. The engineered nanomaterials give enormous yield. The impact of these nanomaterials on the human health and environment is very little known by us. Even recognized nanomaterials, e.g., silver may cause a risk when engineered to nano series. Nanoparticles can enter the human body through ingestion and breathing and through the skin. Carbon made fibrous nanomaterials have been shown to provoke impatience in the lungs in ways that are analogous to asbestos [1].

Nowadays, world is facing challenges of energy crisis and environmental pollution. The demand of energy for the world is increasing at an alarming rate. The European “World Energy Technology and Climate Policy Outlook” (WETO) predicts that the world need normal growth rate of 2% per annum for the period 2000-2030 for most important energy worldwide. The increasing energy demand has greatly is

producing green house effect and pollutant which is effecting our environment adversely. These reservoirs are diminishing at very high speed and will be diminished soon.

Nowadays, the intensity of CO_2 emissions per capita for emergent nations is 22% of that for the main industrial countries. This will increase significantly as the industrialization increase in these under developed countries. It is estimated that until 2030 more than 50 percent of CO_2 emission will be from the under developed countries [2].

Thus we need a long term solution to meet these challenges in upcoming future. However, it is not enough to generate some energy alternatives but there is also a need of preventing the pollution that is an outcome of the consumption of energy means. Natural gas is a best available alternative for shorter time but to meet long term fuel demands, we have methanol and hydrogen which can be derived from renewable energy resources [3]. Hydrogen is a dirt free energy resource. Hydrogen produces energy by combustion or fuel cells. Now a days nanocomposites of Solar cells have been produced which directly convert chemical energy into electricity with high efficiency as compared with hydrogen combustion engine. They are being developed to be used in transportable, electronics, and mobile devices [4].

Thus emerging trend suggests that to achieve pollution free atmosphere and sustainable conversion of energy, solar cell technology is an excellent means to address all these issues. The use of fuel cell can facilitate us with its efficiency and dependability as well as it reduces the ecological impact by creating environment friendly by-products while using renewable fuel sources, with its unique operating characteristics it can give power production ranging from a few watts to megawatts [5], it can be used for stationary power, transportation and portable electronics [6].

1.2 Background of Nanotechnology

1.2.1 Nanotechnology of the Past

Even long before the start of “nanoera”, peoples were coming across various nanosized objects and the related nano level processes, and using them in practice. However, intuitive nanotechnology antiquities developed spontaneously, without due understanding of the nature of these objects and processes e.g, the fact that small particles of various substances possessed properties different to those of the same substances with larger particle size was known for a long time, but the reason for this was not clear. Thus, people were engaged in nanotechnology subconsciously, without guessing that they were dealing with the nanoworld phenomena. In many instances

secrets of ancient nano production simply passed from generation to generation, without getting into the reasons why the received materials and products derived from them acquired their unique properties [7].

BC people knew and used natural fabrics: flax, cotton, wool, silk. They were able to cultivate them and process into products. What makes these fabrics special is the fact that they have a developed network of pores with the size of 1 to 20 nanometers, i.e., they are typical nanoporous materials. Due to their nanoporous structure natural fabrics possess high utilitarian properties: they absorb sweat well, quickly swell and dry. Since ancient times people mastered the ways of making bread, wine, beer, cheese and other foodstuffs, where the fermentation processes on nanolevel are critical [8].

In Ancient Egypt it was rather common to dye hair in black. For a long time it was believed that the Egyptians used mainly natural vegetative dyes - henna and black hair dye. However, recent research into hair samples from ancient Egyptian burial sites, conducted by Ph. Walter showed that hair was dyed in black with paste from lime, lead oxide and small amount of water. In the course of the dyeing process nanoparticles of galenite (lead sulfide) were formed. Natural black hair color is provided with a pigment called melanin, which in the form of inclusions is spread in hair keratin. The Egyptians were able to make the dyeing paste react with sulfur, which is part of keratin, and receive galenite particles a few nanometers in size, which provided even and steady dyeing [9].

The British museum boasts Licurg's bowl as part of its heritage – an outstanding product of glass makers of Ancient Rome. This bowl, on which Licurg, the tsar of Edons, is depicted, possesses unusual optical properties: it changes color with change of location (inside or outside) of the light source. In natural light the bowl is green, if illuminated from within, it turns red. The analysis of fragments of the bowl, carried out in the laboratories of General Electric in 1959 for the first time, showed that the bowl consists of usual soda-lime-quartz glass and has about 1% of gold and silver, and also 0.5 % of manganese as components. Later, when research techniques became more advanced, scientists discovered nanoparticles of gold and silver from 50 to 100 nm in range using an nanoscience, electronic microscopes and nanotechnology [9]. These particles which are responsible for the unusual coloring of the bowl. In the review on plasmons, published in 2007 in the "Scientific American" magazine, H.A. Atwater explained this phenomenon by effects of plasma excitation of electrons with metal nanoparticles. In the Middle Ages, the engineering of manufacturing of multi-colored church stained-glass windows in Europe achieved high perfection. As the recent research shows, the windows

contained additives of gold and nanoparticles of other metals. In the days of crusades the European knights faced the extraordinary strength of blades in fights against Muslims for the first time, made of an ultra strong Damask steel. All attempts of armoring of medieval Europe to replicate such steel had no success. In 2006 P. Paufler carried out the research of sabre fragments made from the Damask steel using an electronic microscope. The results showed that the steel had nanofibrous structure. It is supposed that such structure was received after a special thermomechanical processing of steel which was made from the ore of special structure [10].

1.3 Solar Energy

The sun is the major source of energy for the residents of earth. The total consumption of energy in one year in the world is equal to the energy striking the earth face in one hour [11]. Another estimate suggests that the solar energy falling on the earth in 30 sunny days is equivalent to the energy created from all fossil fuels on earth, either consumed or unexploited. There are also some issues which bound the use of solar energy. But in spite of all limitations, technical potential for converting sunlight into electricity or heat is approximately calculated as about four times of the total energy utilization on earth [12].Solar cells therefore have the potential to ensure the revolutionary transformation of present global energy situation to a reliable and sustainable energy delivery scheme for the twenty first century. It may provide environmentally benign energy with no emissions and would improve energy safety because of its universal accessibility. Augmented by improved energy efficiency practices and other renewable energy technologies, photovoltaics may be envisioned as a key energy technology in the forthcoming decades.

1.4 History of Solar Cells

Solar photo voltaic cell deals with the conversion of solar energy directly into usable electric power by employing solar cells. In 1839 E. Becquerel discovered photo voltaic effect. Later, Chapin, Pearson and Fuller of Bell Telephone Laboratories for the first time confirmed crystalline silicon based workable solar electricity production after more than hundred years. This was the beginning era of commercial photo voltaic. Since then a steady and substantial growth in this technology has been observed mainly due to government subsidies and incentives. However, during the past two decades a booming growth in the photovoltaic industry occurred because of economic volatility due to an increase in oil prices worldwide and raising awareness about environmental impacts of conventional energy technologies.

Despite all this progress and the inherent potential of photovoltaics, the current share of photovoltaics in global energy production is very low; the cost per Watt-peak of electricity produced being the most important daunting factor. The price of standard PV modules is currently around 3 €/W, which is significantly higher than conventional electricity generation technologies. However, different studies have established that this cost may potentially be lowered to 2 €/W by 2010, 1 €/watt till 2020 and till the end of 2030 further cost reduction to the level of 0.5 €/W is expected. Even after 2030, a further price reduction is also expected [12]. Major factors contributing to this cost reduction are continued market growth, superior production strategies, improvement in solar module efficiencies and technological developments in this area [13].

1.5 Resources of Energy and Solar Cells

Currently employed power production technologies are based on fossil fuels (oil, coal or natural gas), nuclear reactors and hydroelectric power projects. Emerging technologies like solar thermal and solar photo voltaics, wind power, bio fuels and tidal energy have demonstrated significant potential as well. At present, electricity all over the world is mainly produced by burning natural gas, oil and coal [13]. Nuclear power production is the second leading source of electricity generation in technologically advanced countries [14]. Hydroelectric power is another attractive electricity generation technology, especially in developing countries. However, environmental footprints, varying in severity, are associated with all types of energy technologies [15]. These include emission of greenhouse gases especially CO_2 in the atmosphere, production of both long-lived and short lived radioactive isotopes from nuclear reactors and drastic influence on river ecosystem and fisheries as well as dislocation and disruptions caused by large hydropower projects [16].

Besides these environmental aspects, other factors like finite availability and non-equitable distribution of fossil fuels, and issues related to energy security necessitate development of viable, clean, efficient and environmentally benign power generation sources and technologies. Leading options may include: wind energy, solar thermal energy, geothermal solar photovoltaics biomass, ocean energy.

The work described in this thesis deals with solar photovoltaic materials. Therefore, the following sections give some background to these types of materials.

1.6 Types of Solar Cells

Table 1.1: Types of Fuel cells

S. No.	Types	Comments	References
1	Buried Contact Solar cell	UNSW developed these buried contact solar cells in 1984.	[17]
2	Cadmium telluride solar cell	Cadmium telluride solar cells were developed to convert solar energy into electrical energy.	[18,19]
3.	Dye-sensitized solar cell	Dye-sensitized solar cells are very efficient and low costs solar cells.	[20]
4	Hybrid solar cell	Hybrid solar cells have conjugated polymers made of organic materials. These conjugated polymers transport holes as sun energy falls on it. The sun energy acts as donor impurity.	[21]
5	Mono crystalline solar cell	Mono crystalline solar cells are made of silicon. These silicon atoms have crystal type structure.	[22]
6	Quantum dot solar cell	Quantum dot solar cells are the most advanced solar cells which uses quantum dots. These quantum dots absorb sun light energy which is then converted into solar energy indium gallium selenide. These solar cells are more efficient than bulk materials.	[23]
7.	Thin film solar cell	The range of thickness of these materials are upto 10 micrometers from a few nanometers. These solar cells have thin films photovoltaic materials which are deposited on materials. These materials then absorb light and convert it into solar energy.	[24]

1.7 Fundamentals of Photocatalysts

Current developments in the colloidal synthesis of nanomaterials have opened up promising avenues in research for the development of low-cost next generation solar cells with higher power conversion efficiency. Development of safe, simple and straightforward techniques for solution phase synthesis of nanoparticles have boosted the development, fabrication and even commercialization of new photovoltaic devices [25]. These techniques have demonstrated significant potential for yielding fairly monodispersed, well passivated, non-aggregated semiconductor nanocrystals. Additionally, high quality nanomaterials with superior optoelectronic properties are being explored to develop photovolatic devices. In order to lower the fabrication cost of the light absorbing layer of the solar cells, one approach involves using colloidal semiconductor nanocrystals as photo-absorber 'ink'. Either electronically coupled arrays of nanocrystal are cast onto a substrate or bulk semiconductor layers of nanocrystals are developed by sintering and thus a desired bandgap of the absorber material is obtained for harvesting the solar radiations spectrum in an efficient and effective manner [26].

Although the sintered and nanocrystals array devices are less than 37% efficient in power conversion (i.e. the Shockley–Queisser limit). Solar cells and modules can be produced at significantly lower cost. In fact, this approach yields more cost effective solar cells and solar modules than corresponding vacuum based methods for photo absorber layer deposition. Discovery of "carrier multiplication" or "multiple exciton generation" in some nanocrystals may give quantum yields greater than 100%. Research efforts are underway to develop solar photovoltaic devices based on these nanoparticles and it is anticipated that such devices may exceed the Shockley–Queisser limit, thus giving rise to a new generation of commercially viable photovoltaic technology. The phenomenon of multiple excitation generation has been studied in colloidal quantum dots of low band-gap materials (0.6– 1.1 eV) like PbS, PbSe, InAs etc. [27,28].

Vacuum based deposition processes, high processing temperatures, longer processing times and expansive precursors as well as substrate materials increase the manufacturing cost of solar cells and solar modules. Consequently, this cost can be significantly decreased by the utilization of solution-phase processes, lower processing temperatures, shorter processing time and cheaper precursors as well as substrates that may permit optimal scale up like 'roll to roll' manufacturing process [29]. The bandgap value of the nanocrystal array or sintered nanocrystal layer is the issue of prime importance in selection of absorber material for Solar cells modules.

Fossil fuel is considered as cheap and relatively inexpensive source of energy in current days. As the consumption of fossils fuel increasing similarly the environmental problems also increasing. Recently in USA the disasters of fossil fuels carrying ship which adversely affect the biological life in the ocean. It has an impact on our environment, economic and health however is inestimable.

Energy issue is now been solve by adopting difficult strategies which has been point out by recent articles in science .For example large area is require for the installation of highly renewable solar cells and wind energies.

Shockley-Queisser photo conversion efficiency can be minimized to 33% for a PV panel. In recent future the new endeavors for nanostructure semiconductor materials design next-solar cells, such as tapping of hot electrons and multiple carrier generation in nanostructures. The theoretical limit can be adjusted to 66%.3. The elementary understanding of light-harvesting assemblies and the charge-transfer processes can be understood through physical chemistry. The organic hybrid solar cells and solar fuels found in literature as nano-structured photocatalyst. The design of next-generation solar cells via semiconductor nanostructures were explored in detail. The main examples were semiconductor nanocrystals or quantum dots, the function for both as light absorbers. The quantum dots like PbSe and CdSe were found appropriate choice for solar cells due to its size-dependent optical and electronic properties, which makes them a suitable candidate for capture hot electrons.

The latest advances regarding the designing semiconductor-sensitized solar cells were reported by Bisquert and Mora-Sero. The dye-sensitized solar cells (DSSCs) provided the same theme of separating photo generated charge carriers. The efficiencies of DSSCs are (~12%) as compared to the semiconductor-sensitized solar cells (4-5%). The further investigation was carried out to discover the new materials for control of recombination, band alignment by surface treatments, counter electrodes, and development of absorbing nanocomposites with enhanced light-harvesting properties.

One more set of solar cells that use semiconductor nanocrystals and polymers to get charge separation under sun light irradiation. The interfacial charge transfer between semiconductor and polymer increases as the optimization of capping agents of semiconductor nanocrystals decreases. The nanoporous TiO2 and an organic hole-transporting material deposited by antimony sulphide have 5.5% efficiency for solar conversion.

Novel methods to design next generation solar cells will be developed to obtain new properties for optical and electronic semiconductors nanocrystals. Fundamental understanding of the charge-transfer kinetics will make advances in semiconductors nanocrystals based solar cells.

1.8 Solar Nanocomposites

Solar nanocomposites are electrochemical device which generates electric current when sun energy strikes to these nanocomposites. Pure nanoparticles of antimony sulphide were prepared and these nanoparticles were doped by cadmium metal which shows a considerable decrease in the energy band gap of these nanoparticles which is confirmed by different characterization techniques. So as the amount of cadmium increases energy band gap decreases and these nanoparticles can be used in solar cells technology.

Procedure for the synthesis of antimony sulphide nanoparticles and its doped forms all the chemicals used were of analytical grade and used without purification. Deionized water was used throughout the experiments. Following method were used for the synthesis of these nanoparticles and its doped forms.

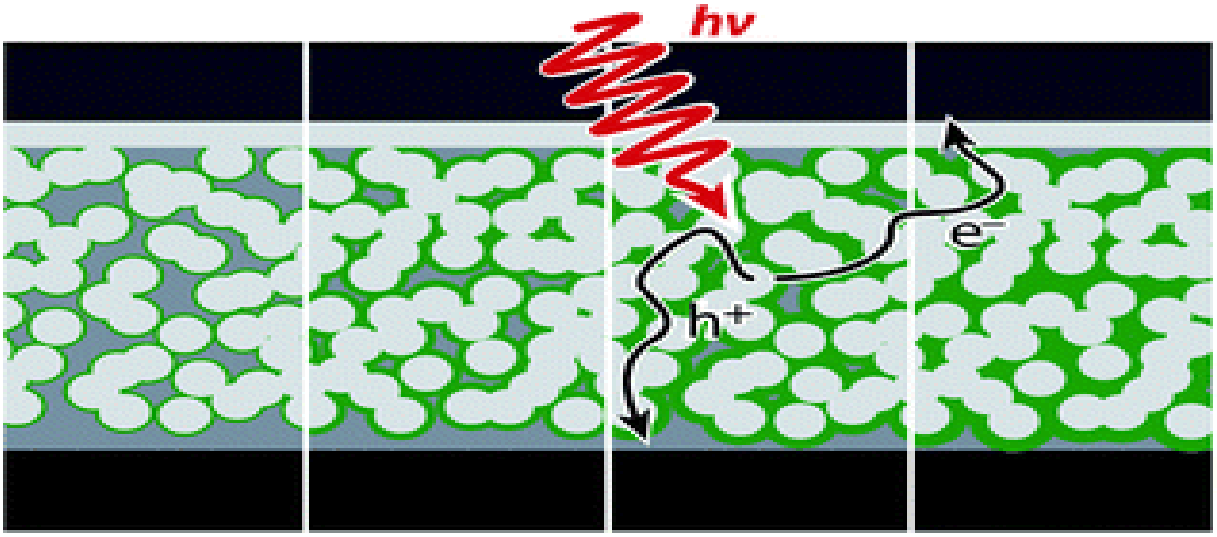

Figure 1.1: Shows how antimony sulphide photocatalysts work

1.9 Mechanism of Photocatalysts

When radiation from sunlight strikes nanoparticles photocatalysts of titanium dioxide (TiO2) a, it produces pairs of holes and electrons. When light strikes titanium oxide the valence bonded electrons become excited. Then this electron is promoted to the conduction band which produces a negative electron and a positive hole pair. It is referred as the semiconductor's 'photo-excitation' state. This difference between energy

the conduction and valence is called 'Band Gap'. The wavelength of the light used for photo-excitation is 388 nm. The figure 1.2 shows how these photocatalysts work.

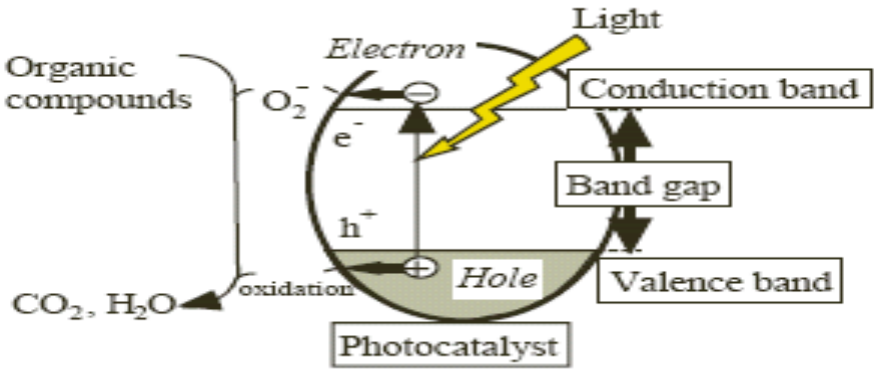

Figure 1.2: Mechanism of Photocatalyst

Until light is available this cycle continues. The electron which has negative charge reacts with oxygen to form an anion of super oxide. The titanium dioxide which has positive hole reacts with water to produce hydrogen gas and hydroxyl radical.

Despite all this progress and the inherent potential of photovoltaics, the current share of photovoltaics in global energy production is very low; the cost per Watt-peak of electricity produced being the most important daunting factor. The price of standard PV modules is currently around 3 €/W, which is significantly higher than conventional electricity generation technologies. However, different studies have established that this cost may potentially be lowered to 2 €/W by 2010, 1 €/watt till 2020 and till the end of 2030 further cost reduction to the level of 0.5 €/W is expected. Even after 2030, a further price reduction is also expected [29].Major factors contributing to this cost reduction are continued market growth, superior production strategies, improvement in solar module efficiencies and technological developments in this area [30].

1.10 Solar Photovoltaic Technologies

A PV system consists of solar cells and these cells arrayed together constitute a solar module for generating the electricity. Other important components include the cabling, battery, charge controller, DC/AC inverter and other support components. The most important component of the solar cell is the light absorbing semiconductor material which absorbs photons of light to produce electron and hole carriers via the photovoltaic effect. Current PV market relies on various technologies employing wafer based silicon and some thin film technologies, which may be categorized as first generation and second generation technologies. Figure 1.3 represents current share of various PV technologies in global PV market.

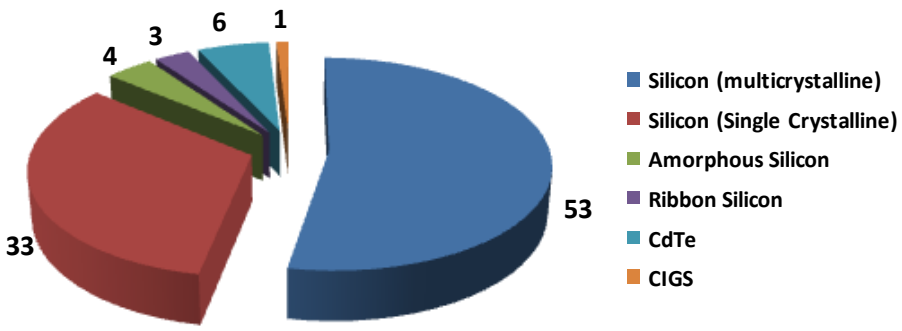

Figure 1.3: Current market share of various PV technologies

First generation PV technologies are based on silicon wafers having maximum power conversion efficiencies of ~ 25% and ~ 13-15.5%, for single crystalline and multi-crystalline silicon wafer based cells, respectively [31,32]. Around half of the cost involved in first generation PV technologies is the material cost for silicon wafers as it requires high quality feed stock and much silicon is lost during processing. Furthermore, above 30% increase in PV manufacturing during recent years has now resulted in more excessive demand for silicon feedstock than supplies, thereby causing significant increase of its costs. Therefore, it is likely that cost reduction trend for first generation PV technologies will reach its limits before they reach full-cost competiveness [33].

Second generation PV technologies are single junction devices that present the key advantage of reduced material use and thus reduced associated costs, while still maintaining the efficiencies analogous or better than first generation PV technologies. In this approach, thin layers of semiconductors like amorphous, polycrystalline, microcrystalline or nanocrystalline silicon, cadmium telluride (CdTe), Antimony sulphide and chalcopyrite compound semiconductors like copper are deposited on less costly substrates like glass. Semiconductor materials used in these technologies have high solar optical absorption coefficients (greater than 10^5/cm). Therefore, absorber film thickness is typically less than a micron and 100-1000 times lesser materials than silicon wafers-based PV are required. Besides, it makes it possible to manufacture thin film solar cell modules as expanded units. Large scale production, thus offers even better economy of scales [34, 35].

Efficiencies obtained so far for second generation PV technologies are low. Highest stabilized efficiencies for amorphous silicon, micro- or nanocrystalline silicon and polycrystalline silicon are ~ 9.5 %, [36] 13%, [37] and 10.4%, [38] respectively.

Similarly, maximum power conversion efficiencies of ~ 16.7%, [39] and 19.4% [40] have been reported for cadmium telluride (CdTe) and copper indium gallium diselenide based solar cells.

Third generation photovoltaics covers a range of budding devices, upstarts, and emerging ideas that have joined the race for achieving requisite performance and cost targets for delivering 15-30 terawatts of solar power by mid-century [41]. No clear definition of the term third generation exists. Whereas second generation technologies might be competing silicon wafer based technologies in the near term, third generation technologies have yet to undergo a marathon struggle to demonstrate their applicability and bring them to commercialization [42]. Notable development has been made, especially in mountain bike or multi-junction devices, dye-sensitized solar cells, quantum dot solar cells and organic solar cells with an efficiency of 32 ± 1.5 has already been reported for GaInP/GaAs/Ge multi-junction devices under global AM 1.5 spectrum [43]. Even higher efficiencies of ~ 40% have been verified for multi-junction or tandem cells with concentrators.

1.11 How Antimony Based Photocatalyst Act in Solar Cell

Extremely thin absorber (ETA) solar cells are nanostructured all-solid photovoltaic devices in which light absorption occurs in a thin intrinsic layer. In this work, ETA cells are built in which an Sb_2S_3 light absorber coating is created by atomic layer deposition (ALD). A model system based on flat layers of ITO, TiO_2, Sb_2S_3, CuSCN and Au is assembled first. The external quantum efficiency (EQE) spectrum follows the absorption spectrum of Sb_2S_3. The EQE depends on the light absorber thickness and on the light intensity in a very non-linear manner. In nanostructured cells based on colloidal, nanocrystalline TiO_2, we show subsequently that Sb_2S_3 can be deposited by ALD homogeneously along the depth axis and that it is free of oxide. Furthermore, the Sb_2S_3 layer thickness can be optimized systematically. In our geometry, we find an optimal thickness of 10 nm, which yields efficiencies of up to 2.6%.

Antimony sulfide (Sb_2S_3) are semiconductors with interesting thermoelectric properties. The direct band-gap of antimony sulfide is 1.78–2.50 eV, and it has interesting high photosensitivity and high thermoelectric power. The band gap covers the visible and near infrared range of the solar spectrum energy, making it potentially useful in solar energy conversion, thermoelectric cooling technologies and optoelectronics in the IR region [44].

1.12 Background Semiconductor Theory

An insight into properties at an atomic level is required in order to fully know the electronic properties of semiconductors. Band theory represents a common approach utilized to explain the original properties of semiconductors. This originates from molecular orbital theory in which the linear combination of atomic orbitals approximation is used to describe the formation of molecular orbitals on the beginning of interaction of wavefunctions. In a simple case of hydrogen, the single s electron wavefunctions of two hydrogen atoms (commonly represented as χ_A and χ_B) interact in all possible linear combinations to produce a bonding and antibonding orbital (ψ_1 and ψ_2 respectively):

$$\psi_1 = \chi_A + \chi_B$$

$$\psi_2 = \chi_A - \chi_B$$

The molecular orbitals thus formed are having differing energy levels than the corresponding atomic s orbitals. The bonding orbitals have lower energy than the original atomic energy levels while the antibonding orbitals are higher in energy than the original atomic energy levels. The two s electrons from hydrogen atoms A and B in this case reside in the lowest possible energy configuration therefore populating the bonding orbital whereas the antibonding orbitals stay behind unoccupied [45].

In a similar way, bound electrons in an individual atom have discrete energy levels separated by forbidden energy regions while in solids, the distinct levels broaden to form allowed bands which are separated by bandgaps. Band theory can be used to explain these continuous bands of energy levels displayed in solids. This continuous band is caused by the negligible energy gap between the molecular orbitals arising from the interaction of wavefunctions of atomic orbitals. It is possible for the energy states within each band to be occupied by pairs of electrons (according to the Pauli's exclusion principle). Electrons will reside in the lowest energy levels at absolute zero, commonly called the valence band while the higher energy levels termed as the conduction band remain unoccupied at absolute zero temperature. Electrons are not capable to occupy the region in between these energy bands and this region is termed as the band gap (E_g). Absorption of sufficient energy, results in transition of an electron from the valence band that crosses the band gap and shifts to the conduction band. The energy required for this transition is characteristic of the particular material in question and these unique band gaps, are generally measured in electron-volts (eV). For conduction to be possible a

partially filled band is required (as a net motion of electrons is required for conduction). More electrons present in the conduction band would mean that the material would be more conductive [46].

The difference in the band gap makes a material either an insulator or semiconductor. Materials with larger band gaps, 9 eV or greater are insulators whereas semiconductors usually have a band gap in the region 0.5-2.0 eV. Therefore in the insulator, no transition of electrons from the valence band to the conduction band is viable, no matter how much external energy is applied to make this transfer. This thus means no conduction is possible in these types of materials, as electrons are not likely to populate a partially occupied conduction band, and hence the term "insulator" is used for such materials. The opposite is true for a metallic conductor, where the valence and the conduction bands overlap each other meaning there is essentially no band gap present. This means that even at low temperatures, there is continuous transfer of electrons from the valence band to the conduction band. Therefore, the electrons in metallic conductors have enough freedom to move about the lattice.

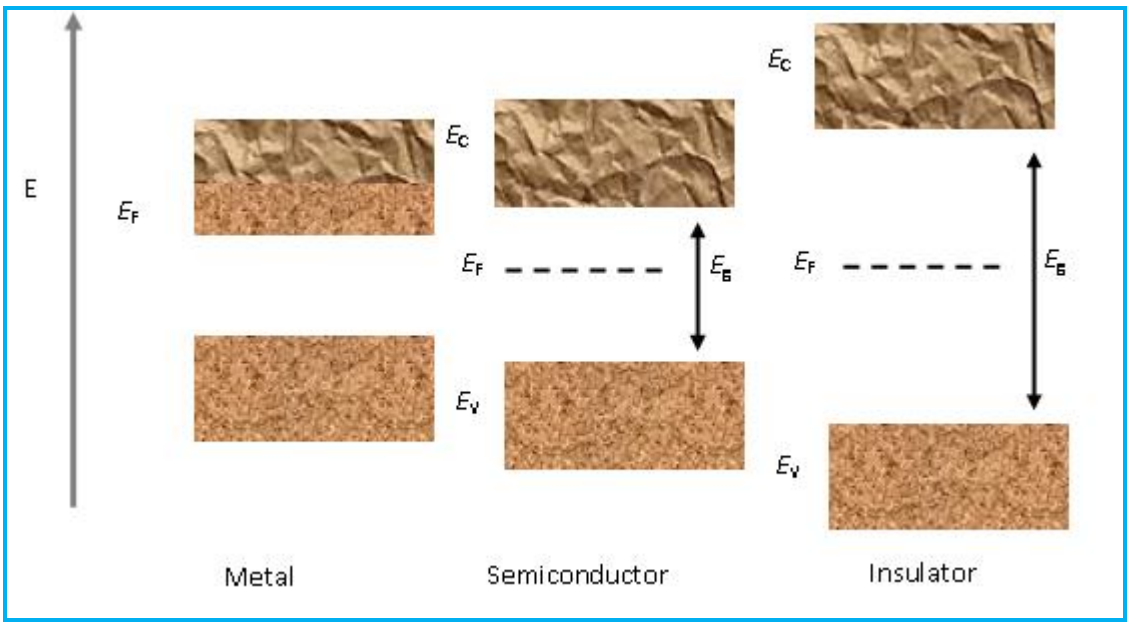

Figure 1.4: Schematic illustration of typical band diagrams for a metal, an intrinsic semiconductor and an insulator.Ev represents the energy linked with valence band while Ec represents the energy associated with the conduction band.

Semiconductors possess a band structure that is intermediate between that of insulators and metallic conductors. At absolute zero temperature, all electrons of the semiconductor matter occupy the lower energy valence band while conduction band remains unoccupied. However, at finite temperatures, the band gap is significant but is well less than that of insulators. At low temperature, electrons mostly occupy the valence band with little or no electrons in the conduction band. Therefore at low temperature there is little, if any, conduction. While at higher temperature, electrons have enough energy to get promoted to the conduction band via the band gap thus building the conduction possible [47].

For molecules, the quantity of molecules inhabiting a particular energy level at a particular temperature can be calculated using the Boltzmann distribution, but in the case of electrons in semiconductors, Fermi-Dirac distribution function is used to calculate occupation statistics of energy levels. This means that Fermi-Dirac distribution gives the probability of an electron occupying a particular energy band in semiconductors at a known temperature:

$$f(E) = 1 + \exp[(E-E_f)/K_bT]$$

This relationship suggests that an exponential relationship exists between the temperature and the probability of occupancy. The chances of electrons being promoted to the conduction band increase extensively with an increase in the temperature (i.e. increases the chances of electrons appearing above the Fermi level). Therefore, this expression clearly suggests an increase in conductivity of semiconductors with a rise in temperature. Theoretical curves of the Fermi-Dirac distribution function given in Figure 1.4 clearly reveal this phenomenon. Figure 1.5 shows part of the photoelectron spectrum of ruthenium at three different temperatures, with the theoretical curves of the Fermi-Dirac distribution function superimposed (as the smooth line) [48]. A very strong correlation between the theoretical curves and experimental curves is clearly obvious from this figure.

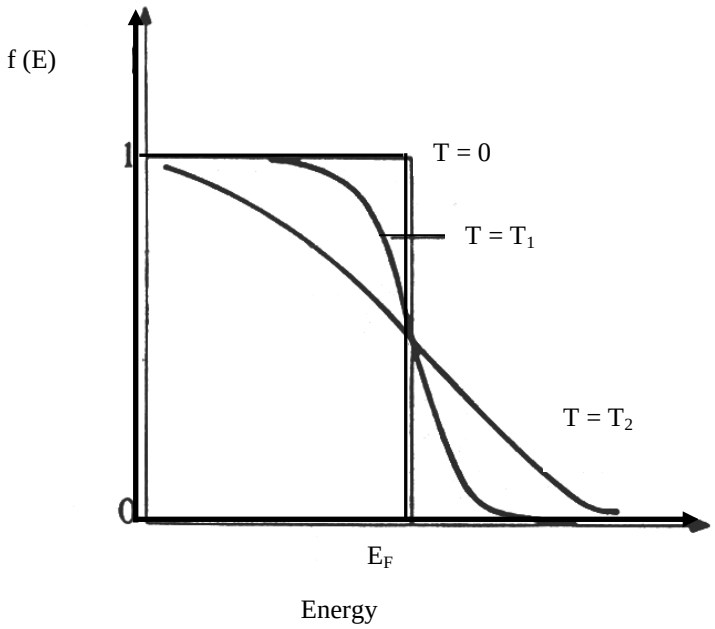

Figure 1.5: Fermi-Dirac distribution function. Theoretical curves at 0 K (T=0), and two higher temperatures where (T_2>T_1>0)

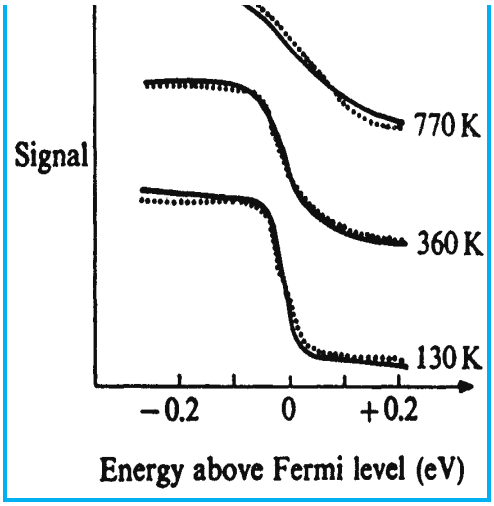

Figure 1.6: Part of the photoelectron spectrum of metallic ruthenium at three different temperatures. The smooth line is theoretical and the dotted experimental

1.12.1 Direct and Indirect Bandgap Semiconductors

An important factor determining the efficiency of absorption of light photons in a semiconductor absorber and electron-hole pairs generation is known as the absorption coefficient. When transitions of electrons from the valence band to the conduction band occur in semiconductors, a change in crystal momentum (k, wavevector) may or may not occur. This occurrence of change in k, wavevector depends on the possible route available involving lowest energy transition. In a typical absorption process, an electron is excited from the valence band to the conduction band upon absorption of a photon.

This absorption process occurs with conservation of both the energy and the momentum. The momentum of photon being so small in comparison with the momentum of crystal, electron's momentum should essentially be conserved in the absorption process. If the minima of the conduction band and the maxima of the valence band occur at the same value of the wave vector k (Figure 1.7a) in a transition, such transitions are called direct transitions, and the material is termed a direct band gap semiconductor.

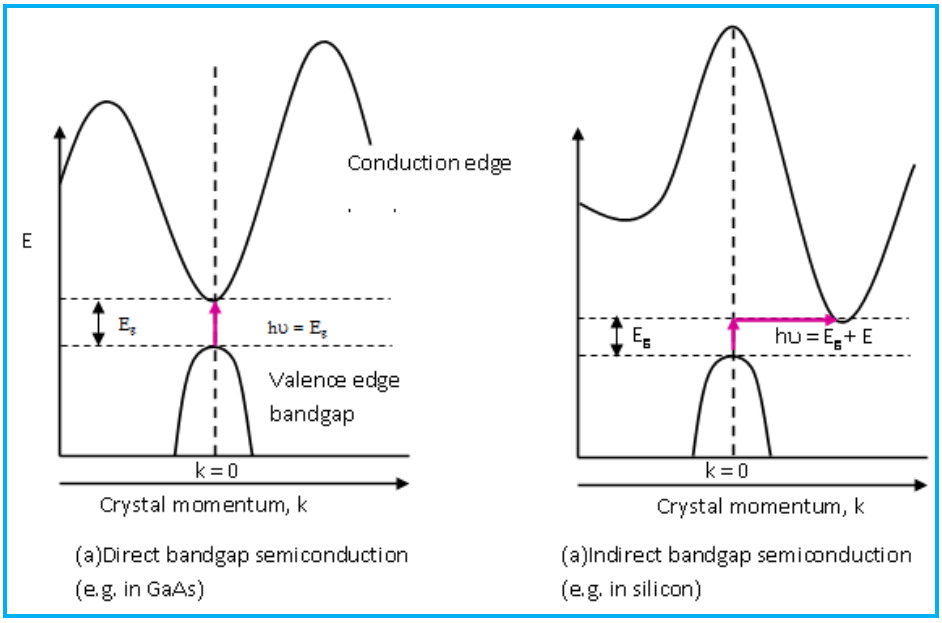

Figure 1.7: Energy band diagram for direct and indirect semiconductors

Transitions are referred to as indirect transitions if they involve a state in which band extrema occur at different values of wavevector k, (Figure 1.7b) and accordingly the material is referred to as an indirect band gap semiconductor. Another particle i.e. a phonon is needed for momentum conservation in such transitions. As compared to direct transitions, the probability for indirect transitions is significantly lower. Therefore, relatively weaker fundamental absorption generally occurs in indirect band gap materials as compared to direct band gap materials. This means that before absorption, a photon is compulsory to travel a extensive distance into the material there by restrictive the chances of such transitions. Therefore, direct band gap materials have much higher probability of the absorption of photons and therefore possess higher absorption coefficients than indirect band gap materials [49]. Direct transitions, may have values of absorption coefficients varying from 10^4 to 10^5 cm^{-1} while the similar may differ from 10 to 10^3 cm^{-1} for indirect transitions.

1.12.2 Intrinsic Semiconductors

An ideal intrinsic semiconductor is an impurity free semiconductor having no lattice defects in the crystal (e.g. pure silicon). Such semiconducting materials show increased conductivity with increased temperature. An intrinsic semiconductor at T = 0 K, has completely filled valence band energy states while in the conduction band, there are all empty energy states. The Fermi energy must, therefore, be somewhere between E_c and E_v. With the rise in temperature above 0 K, the valence electrons gain thermal energy. As soon as sufficient energy level is achieved, few electrons in the valence band traverse the bandgap and are promoted to the conduction band. Such transition results in generation of an empty state or hole in the valence band.

In an intrinsic semiconductor, thermal energy plays a key role in generating electrons and holes in pairs; thus an equal number of electrons in the conduction band and holes in the valence band are created. The resulting conduction is the result of motion of electrons as well as positively charged holes in the conduction band. Effectively, this can be seen as the two bands now being more partially filled than they were before, hence allowing more conduction.

At any given temperature:

$n(T) = p(T) = n_i(T)$

Where n(T) is the number of electrons in the conduction band, p(T) is the number of holes in the valence band, and n_i is the intrinsic free carrier concentration. Examples of elemental intrinsic semiconductors are silicon and germanium whereas compound intrinsic semiconductors are gallium arsenide, indium phosphide and zinc sulfide and antimony sulphide.

1.12.3 Extrinsic Semiconductors

Though intrinsic semiconductors are of extraordinary interest in academic research, the true strength of semiconductors is manifested by extrinsic semiconducting materials. All commercially available semiconductors are extrinsic which are different from intrinsic semiconductors only due to the presence of intentionally added impurity which changes whole scenario in context of the electronic properties of the material. This process of introducing controlled quantity of impurity is known as doping. There are two types of doping and an extrinsic semiconductor will either be electron donor (n type) or electron acceptor (p type), thus the resulting material will be electron rich or electron deficient. At room temperature relatively high conductivities may be obtained for extrinsic semiconductors as the doping significantly changes the band structure.

Therefore, extrinsic semiconductors can be fabricated in a form, useable in electronic devices at ambient temperatures.

In a semiconductor, doping causes an electronic discontinuity within the lattice which is compensated by the induction of additional energy levels within the band gap. Figure 1.6 represents the band diagram for extrinsic semiconductors of n-type and p-type. If the semiconducting material is doped with an electron donor atom like phosphorus or arsenic, the non-bonding electron in dopant atom is loosely held by weak electrostatic forces. Therefore, at finite temperatures (even at room temperature), thermal energy is sufficient enough to cause transition of electrons to the conduction band, from the valence band. Now a conduction band electron is able to move within a crystal generating a current, while the positive ion remains fixed in the crystal. An electron is therefore donated by such an impurity atom to the conduction band and hence it is called as a donor impurity. It causes an increased number of free electrons in the conduction band than the number of holes present in the valence bond. Such a material is termed as n-type extrinsic semiconductor. Electrons by virtue of their concentration are majority carriers in n-type materials whereas the holes are minority carriers. The Fermi level, for n-type semiconductors, is raised within the bandgap i.e. near to the conduction band. The fermi level's exact position would however, be a function of both the temperature and the donor concentration.

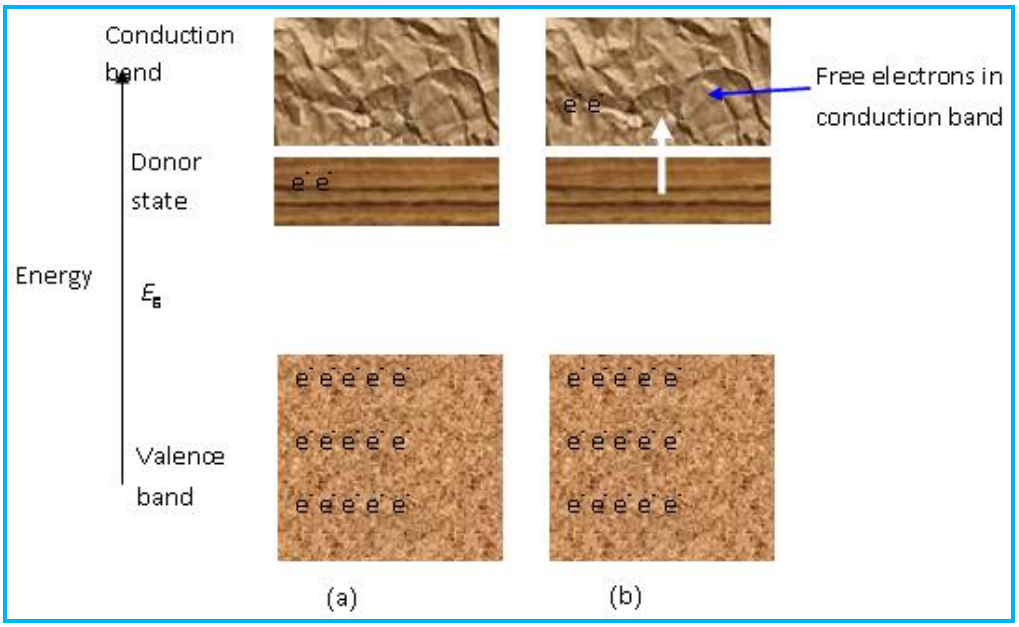

Figure 1.8: Electron Diagram diagrams representing (a) a donor impurity located within the band gap and just below the conduction band; (b) Subsequent excitation of the electron from the band gap to the conduction band.

When the semiconductor atom is substituted by an impurity containing one electron less than the semiconductor atom, this impurity used for doping the semiconductor is called an acceptor (see figure 1.8). Such an impurity introduces an energy level within the bandgap, located near the top of the valence band as the Fermi level. Thermal excitation of an electron from the valence band into the impurity acceptor level creates a positively charged hole. No free electron is created in either the impurity level or in the conduction band. It is noteworthy that the mobile holes are created in valence bands, while the thermally excited electrons are bound to the acceptor atoms. Such kinds of extrinsic semiconductors are commonly termed as p-type semiconducting materials in which majority carriers are the holes and electrons may be called the minority carriers. The acceptor levels in p-type materials do not display band-like qualities and electrons cannot move around in them (i.e. they are discrete energy levels). Movement of the holes in the valence band contributes to conduction of the material in this case. Movement of the holes in valence band is responsible for conduction abilities of the semiconducting material. A good example of such materials is silicon doped with precisely controlled amount of gallium.

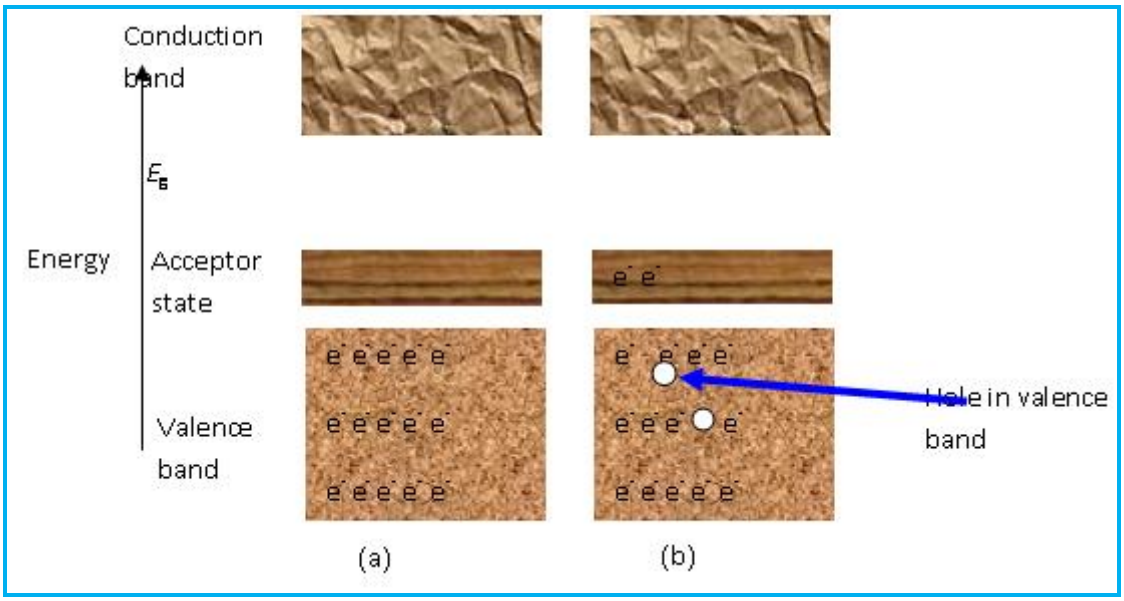

Figure 1.9: Electron band structure for (a) an acceptor impurity level, located within the band gap and lying just above the valence band; (b) excitation of an electron into the acceptor level, leaving behind a positive hole in the valence band.

This may be summarized as in the case of intrinsic semiconductors, the band structure and hence electrical properties solely depend on inherent properties of the pure material and equal concentrations of electrons and holes exist in the material, whereas in the case of extrinsic semiconductors, impurity or dopant alters the band structure and hence dictates the electrical properties of the material. Electron-hole concentrations are not equal in the case of extrinsic semiconductors and depend on the donor or acceptor properties of the dopant used.

1.13 Sb_2S_3 as Semiconductor

As an excellent semiconductor, Sb_2S_3 exhibits important applications in photovoltaic [50], photosensors [51], solar energy and photoelectronics [52,53], optical nanodevices operating in the near-infrared [54].Today, there has been increasing interest in the use of inorganic NPs in different health materials or industrial products such as antimicrobials, catalysts, lubricants and microelectronics instruments. So far, various morphologies and architectures of Sb2S3 nanostructures have been reported, such as hollow cones [55], nanotubes [56], rod-like dendrites [57,58],flake-like and straw-tied-like [59]. Many efficient techniques were developed to prepare nano and bulk Sb_2S_3,mainly including chemical vapor deposition [60], sonochemical [61,62,63], ambient-temperature [64], hydrothermal and solvothermal [65-67], and thermal decomposition methods [68,69].

1.14 Research and Objectives

- Synthesis of antimony sulphide nanoparticles by hydrothermal method
- Characterization of Sb_2S_3 and doped Sb_2S_3 NPs was done
- Doping of Cd in Sb_2S_3 NPs and effect of various concentration of dopant were studied
- Effect of other dopants like Hg and Zn were also studied.

Our objective in this research work is to hydrothermally prepare nanocrystal structures of Sb_2S_3 and metal doped Sb_2S_3 for solar cell applications. The absorber material Sb_2S_3 with band gap of 1.8 eV would not yield acceptable photovoltaic conversion efficiency in bulk whereas the nanocrystalline Sb_2S_3 have band gap of 3.5 eV to 3.7 eV may generate. The ‘ultimate efficiency’ for such an absorber (Sb_2S_3 having band gap 1.8 eV) is about 32% and the ‘detailed balance limit efficiency’ is near 18% according to the Shockley– Queisser analysis. Thus, it would form only a part-absorber; requiring lower band gap materials to supplement the optical absorption. Cd is among the candidates to fulfill this task. Hence they are attractive in the quest for alternative

materials for photovoltaic technologies. Cd, Zn and Hg doped Sb_2S_3 were synthesized and compared with Sb_2S_3 (having band gap 1.8 eV) that if they can be used.

Chapter – 2

EXPERIMENTAL

2.1 Chemicals

The names, formulas, purity and supplier of chemicals are given below in Table.

Table 2.1: Chemicals used for research work

S. No.	Name	Formula	Purity %	M.Wt	Source
1.	Antimony trichloride	$SbCl_3$	99	228 g	Aldrich
2.	Thioglycolic acid	$HSCH_2COOH$	80	92 g	Riedel de Haen
3.	Sodium sulphide trihydrate	$Na_2S.3H_2O$	60	132g	Aldrich
4.	Cadmium chloride	$CdCl_2.2H_2O$	99	219g	Aldrich
5.	Ethanol	CH_3CH_2OH	99	46g	Fluka
6.	Methnol	CH_3OH	99	32g	Fluka
7.	Thioacetamide pure	CH_3CSNH_2	99	75g	Aldrich

2.2 Procedure for the synthesis of Antimony Sulphide Nanoparticles

Hydrothermal method was adopted for the synthesis of antimony sulphide nanoparticles. The water was used as a solvent for the synthesis of antimony sulphide nanoparticles because the presence of water has strong effect on the crystal growth. The procedure is described below.

0.099 gm (0.876mmol) of antimony trichloride and 0.726 gm (15.78mmol) of thioglycolic acid was added into 100 mL of purified distilled water. The solution was stirred for 20 minutes until antimony trichloride was completely dissolved. The reaction mixture was kept under constant magnetic stirring until a clear transparent solution obtained.

The progress of reaction was indicated by the changes in the color of the reaction mixture which becomes a clear transparent solution. After 20 minutes the reaction mixture was transferred to Teflon lined autoclave. The autoclave was then placed in a furnace for 12 hours and the temperature was maintained at 220°C. After 12 hours the reaction was stopped and the autoclave was removed from the furnace. The furnace was cooled and centrifugation was done. The silvery solid precipitate of antimony sulphide nanoparticles were washed five times with distilled ethanol, each time waiting till

complete decantation of antimony sulphide and then throwing away the supernatant ethanol. These thoroughly washed antimony sulphide nanoparticles were stored in the dark [70-74]. :The synthetic scheme for the synthesis of antimony sulphide nanoparticles and its cadmium doped antimony sulphide nanoparticles is given below.

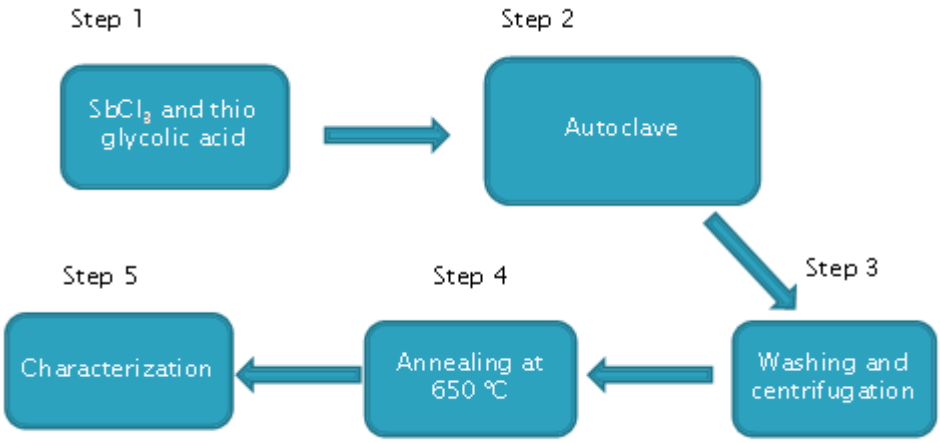

Figure 2.2. Synthetic scheme for Sb_2S_3 nanoparticles and its doped forms.

The whole process can be described by:

$SbCl_3 + H_2O \rightarrow SbOCl + 2H^+ + 2Cl^-$

$2SbOCl + 3HSCH_2COOH \rightarrow Sb_2(HS)_3^{+3} + 3CH_2COOH^+$

$Sb_2(HS)_3^{+3} \rightarrow Sb_2S_3 + 3H^+$

$mSb_2S_3 + KHSCH_2COOH + KSb^{+3} \rightarrow (Sb_2S_3)_m(SbSCH_2COOH)_k^{+2} + KH^+ \rightarrow (m + k)$ Sb_2S_3

According to above mechanism, TGA acts as a soft template; leading to the anisotropic growth of Sb_2S_3along its C-axis [75]. For example, in the growth mechanism of Sb_2S_3 by using complex agent, citric acid can be expressed as the following: first, the Sb^{III} ions cooperate with the citric acid molecules and form the complex ions $[Sb(TSC)_x]^{3-3x}$ and these complex ions dissolve in water [76]. Then, TGA couples cooperate with past complex ions and form a compact structure. By increasing temperature and pressure in hydrothermal treatment, this compact structure degraded and Sb_2S_3 formed. The whole process can be described by:

$SbCl_3 + xTSC^{-3} \rightarrow [Sb(TSC)_x]^{3-3x} + 3Cl^- + 3H^+$

$2[Sb(TSC)_x]^{3-3x} + 3TGA \rightarrow Sb_2S_3 + 2xTSC^{-3} + 3H^+ + 3CH_2COOH^+$

2.3 Procedure for synthesis Cadmium Sulphide doped Antimony Sulphide Nanoparticles

Antimony sulphide nanoparticles were already synthesized in water according to the procedure described above. Then these nanoparticles were doped by different concentration of cadmium chloride salt. These different concentrations of cadmium chloride were $2.5x10^{-3}$g (0.013mmol), $5.0x10^{-3}$ g (0.027mmol), $7.5x10^{-3}$ g (0.040mmol) and $10.0x10^{-3}$ g (0.055mmol) was to antimony sulphide nanoparticles respectively. As the concentration of cadmium sulphide was increased the concentration of antimony sulphide was decreased.

2.4 Changing the ratio between Antimony Sulphide and Cadmium

Antimony sulphide nanoparticles were doped with cadmium by keeping the concentration of antimony sulphide decreasing while the concentration of cadmium was progressively increased to attain the various ratios of antimony sulphide and cadmium (97.5:2.5,95:5,92.5:7.5,90:10) respectively.These different ratio of antimony sulphide doped cadmium were prepared by hydrothermal method and analyzed by different instrumental techniques.

2.5 Characterization Techniques

The prepared nanoparticles were then subjected for characterization by UV-Vis absorption Spectroscopy, X-ray diffraction (powder method), scanning electron microscopy (SEM), and energy dispersive X-ray (EDX) analysis, FT-IR Spectroscopy, and Thermogravimetric analysis(TGA) [77,78].

2.5.1 UV-Visible Optical Absorption Spectroscopy

Energy band gaps (Eg) of the nanoparticles were determined by UV-Visible absorption spectroscopy. A Schmadzu spectrophotometer was used to record the UV-Vis optical absorption spectra of the nanoparticles. The linear dependence of α^2 vs. $h\upsilon$ (α is the absorption coefficient) is indicative of the direct bandgap materials. Extrapolation of the linear region of the absorption plots of α^2 vs. $h\upsilon$ provided band gap values.

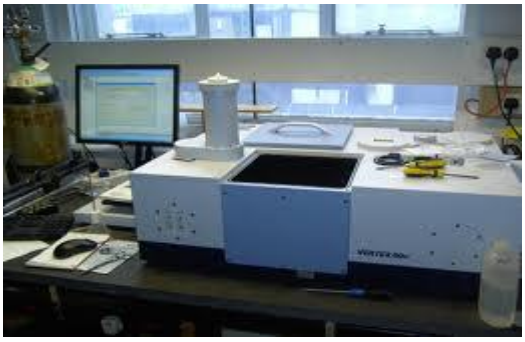

Figure 2.5.1. Image for UV-Visible Spectroscopy.

2.5.2 Powder X-ray Diffraction

Nanoparticles and its doped forms synthesized in this work were characterized by using powder XRD diffraction studies. In the case of nanoparticles, films of nanocrystals were deposited onto glass substrates by simple drop cast method. Bruker AXS D8 diffractometer using monochromated Cu-Kα radiations was used to record XRD patterns. The samples were mounted flat and scanned from 10 to 80 2-theta range with a step size of 0.06 and a count rate of 10 seconds. The diffraction patterns obtained were then compared to the documented patterns in the ICDD database using EVA software package.

The d-spacings were calculated by Bragg's law:

$n\lambda = 2d\sin\theta$

Where λ is the wavelength of the radiation used, n is an integer, d is the perpendicular spacing between the lattice planes in the crystal lattice and θ is the complement of the angle of incidence of the X-ray beam.

Crystallite sizes (normal to planes hkl) were anticipated using the Scherrer formula:

Crystallite size (nm) = $0.9\ \lambda / B \cos\theta$

Where λ is the wavelength of the radiation used, and B is the broadening parameter with reference to a standard sample, defined by $B = (B_M^2 - B_S^2)^{0.5}$, where B_M and B_S are the full width at half maximum (FWHM) of peaks in radians for the measured and standard samples, respectively. Errors were estimated to be of the order ±5%.

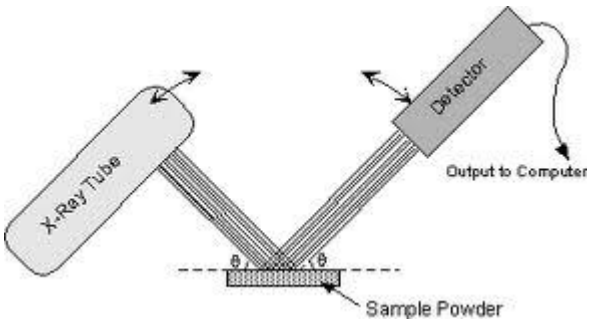

Figure 2.5.2 Schematic diagram for XRD analysis.

2.5.3 Scanning Electron Microscopy (SEM) and Energy Dispersive X-ray (EDX) Analysis

SEM was performed using a Philips XL 30 FEGSEM and EDX analysis was carried out using a DX4 instrument. To keep away from charging of the sample by the electron beam, nanoparticles and its doped forms were carbon coated using Edwards E-306A coating system before carrying out SEM and EDX analysis.

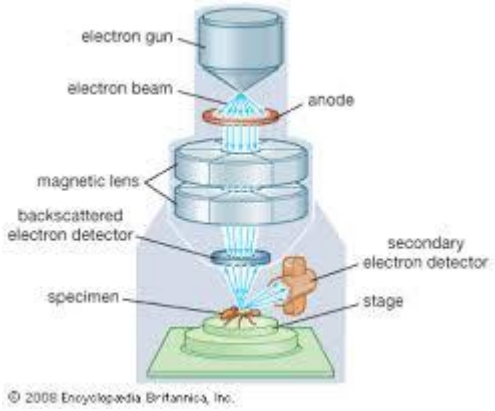

Figure 2.5.3. Schematic diagram for SEM analysis.

2.5.4 Thermogravimetric Analysis (TGA)

Perkin Elmer Differential Scanning Calorimeter 8500 with Thermo gravimetric analyzer 400 (TGA) was used to carried out the thermal analysis of nanoparticles and it's doped forms. It is a method of thermal analysis in which changes in physical and chemical properties of materials are measured as a function of increasing temperature (with constant heating rate), or as a function of time (with constant temperature and/or constant mass loss. It is used for volatile content and water. TGA shows thermal stability of the material.

Figure 2.5.4. Image for TGA analysis.

2.5.5 FT-IR Spectroscopy

FT-IR stands for Fourier Transform Infra Red. In infrared spectroscopy, sample is exposed to infrared radiation. Sample absorbs some radiations leaving some as transmitted radiations. A spectrum is obtained by absorption and emission of radiations by sample. Like a fingerprint, no two different sample produce the similar spectrum. This makes infrared spectroscopy a useful tool for several type of analysis.

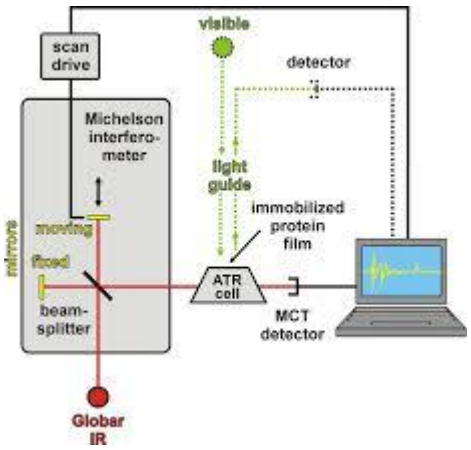

Figure 2.5.5. Schematic diagram for FT-IR analysis.

Chapter – 3

RESULTS AND DISCUSSION

Antimony sulphide and cadmium doped antimony sulphide nanoparticles were synthesized by hydrothermal method using different concentrations of cadmium salt. The synthesized nanoparticles were then characterized by X-ray Diffraction (XRD), Fourier Transform Infrared Spectroscopy (FT-IR), Thermo Gravimetric Analysis (TGA), UV-Visible Spectroscopy, Energy Dispersive X-ray (EDX) and Scanning Electron Microscopy. The comparative studies of the synthesized nanoparticles were carried out as their application in solar cells [79-80].

3.1 X-ray Diffraction (XRD)

X-ray Diffraction technique was used to get information about average crystalline size, phase of nanoparticles and crystallinity of the synthesized nanoparticles. XRD of pure antimony sulphide nanoparticles is shown in figure 3.1 [81] and cadmium doped nanoparticles is shown in figure 3.2 to 3.5. All the characteristics peaks of pure antimony sulphide were present which showed that the material is pure. It also shows that these nanoparticles are highly crystalline. The sharpness of the peaks indicates the change in the crystallinity and size of the nanoparticles. The synthesized nanoparticles had shown different crystallite size depending on different concentrations of cadmium salt for doping. The average crystallite size was calculated by using debye scherrer equation and results are given in Table 3.1.

Table 3.1: Average crystallite size of synthesized pure and doped nanoparticles

S. No.	Sample	Name of Nanoparticles	Average Crystallite size
1.	AS	Pure Antimony Sulphide	31.1nm
2.	AS1	2.5% Cadmium doped Sb_2S_3	34.1nm
3.	AS2	5% Cadmium doped Sb_2S_3	23.1nm
4.	AS3	7.5 % Cadmium doped Sb_2S_3	31.6nm
5.	AS4	10% Cadmium doped Sb_2S_3	52.9nm

The X-ray Diffraction (XRD) results showed that the synthesized pure and doped nanoparticles have different crystallite sizes. As the sharpness of the peaks increases the crystallinity of the synthesized particles also increases, which is clear from the given spectra. The XRD results are shown below.

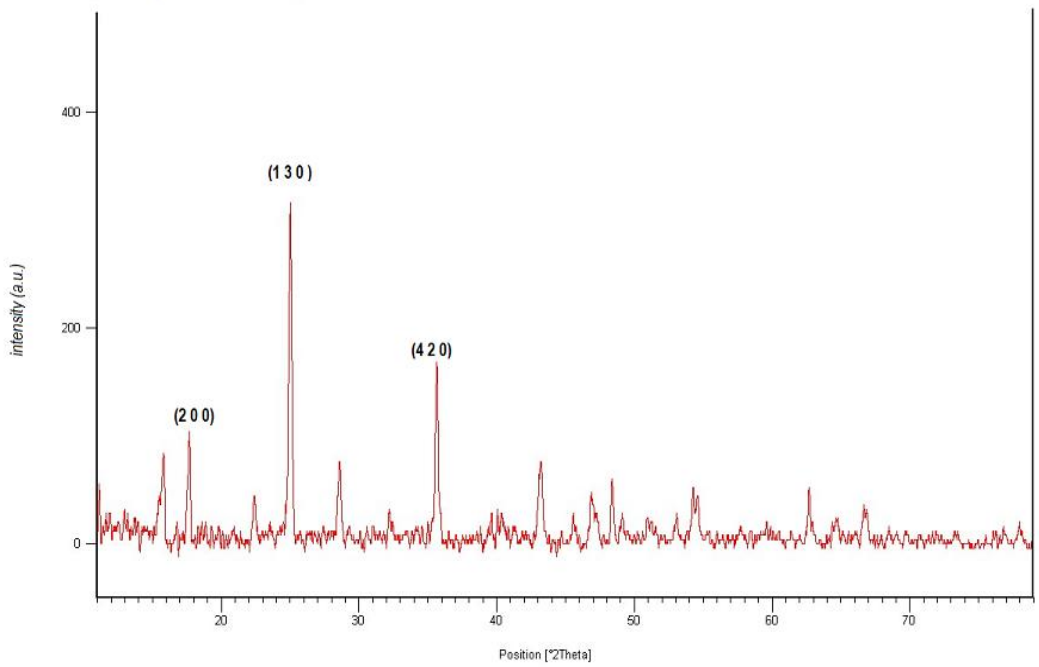

Figure 3.1: XRD pattern of Sb_2S_3 nanoparticles

Figure 3.1 showed the XRD pattern of the prepared antimony sulphide nanoparticles. All the peaks in the pattern can be indexed to the orthorhombhic phase with lattice parameters a =1.122 nm, b=1.228 nm and c=0.384 nm. The intensity and peaks are in good agreement with the values reported in the literature (JCPDS card file :42-1393). No characteristic peaks are observed for other impurities like antimony oxide. The average crystalline size was evaluated from the full width at half maximum (FWHM) of the diffraction peaks at different angles. The estimated average crystalline size was found to about 31.1 nm. The peaks suggested that the antimony sulphide nanoparticles are crystalline.

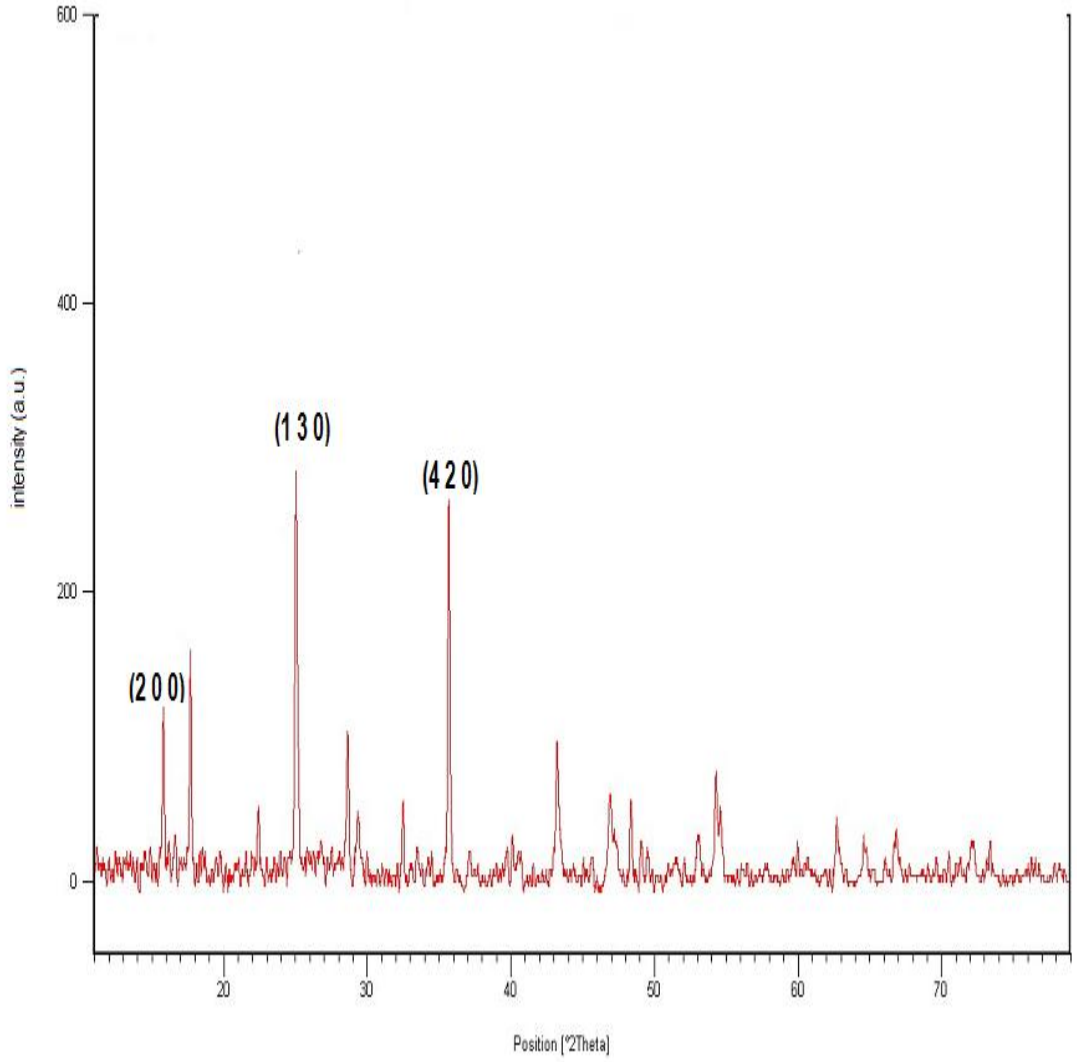

Figure 3.2: XRD pattern of 2.5% Cd doped Sb_2S_3 nanoparticles

The 2.5 percent Cd doped antimony sulphide indicated that the peaks are higly crystalline and the size of the nanoparticles is 34.1 nm. As the crystallinity increased the size of the nanoparticles also increased. No other characteristic peaks were found in the XRD spectrum for elemental cadmium or cadmium sulphide which indicates the doping of cadmium in antimony sulphide nanoparticles.

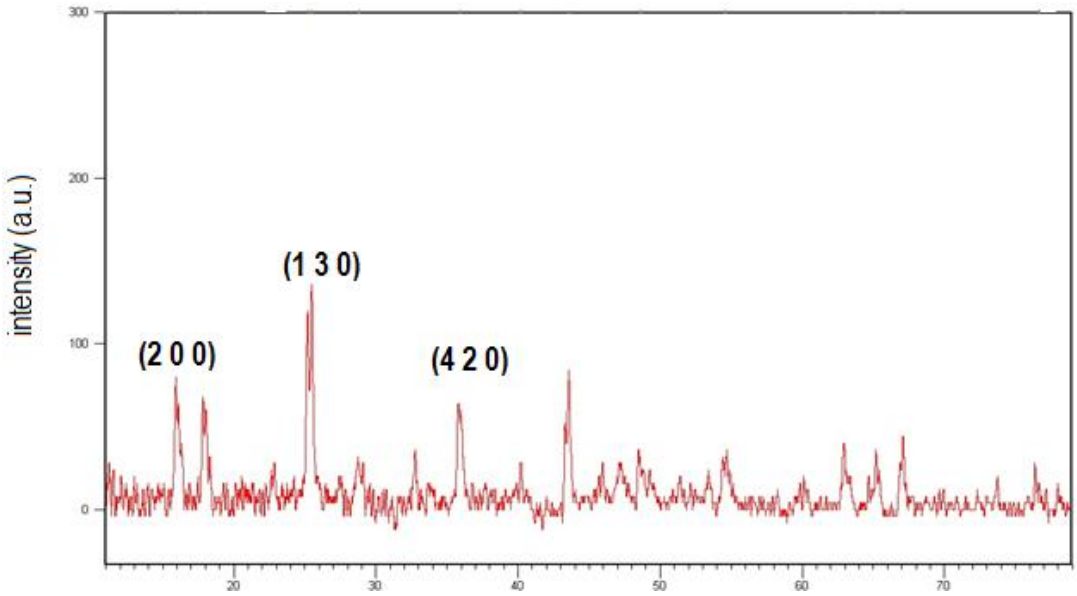

Figure 3.3: XRD pattern of 5% Cd doped Sb_2S_3 nanoparticles

The figure 5 percent Cd doped antimony sulphide indicated that the crystallinity decreases in as a result the size of the nanoparticles also decreases. The average size of the nanoparticles is 23.1 nm. All the characteristics peaks are present in the spectrum and no extra peak is present for impurities like cadmium or cadmium sulphide. It also indicated doping of cadmium.

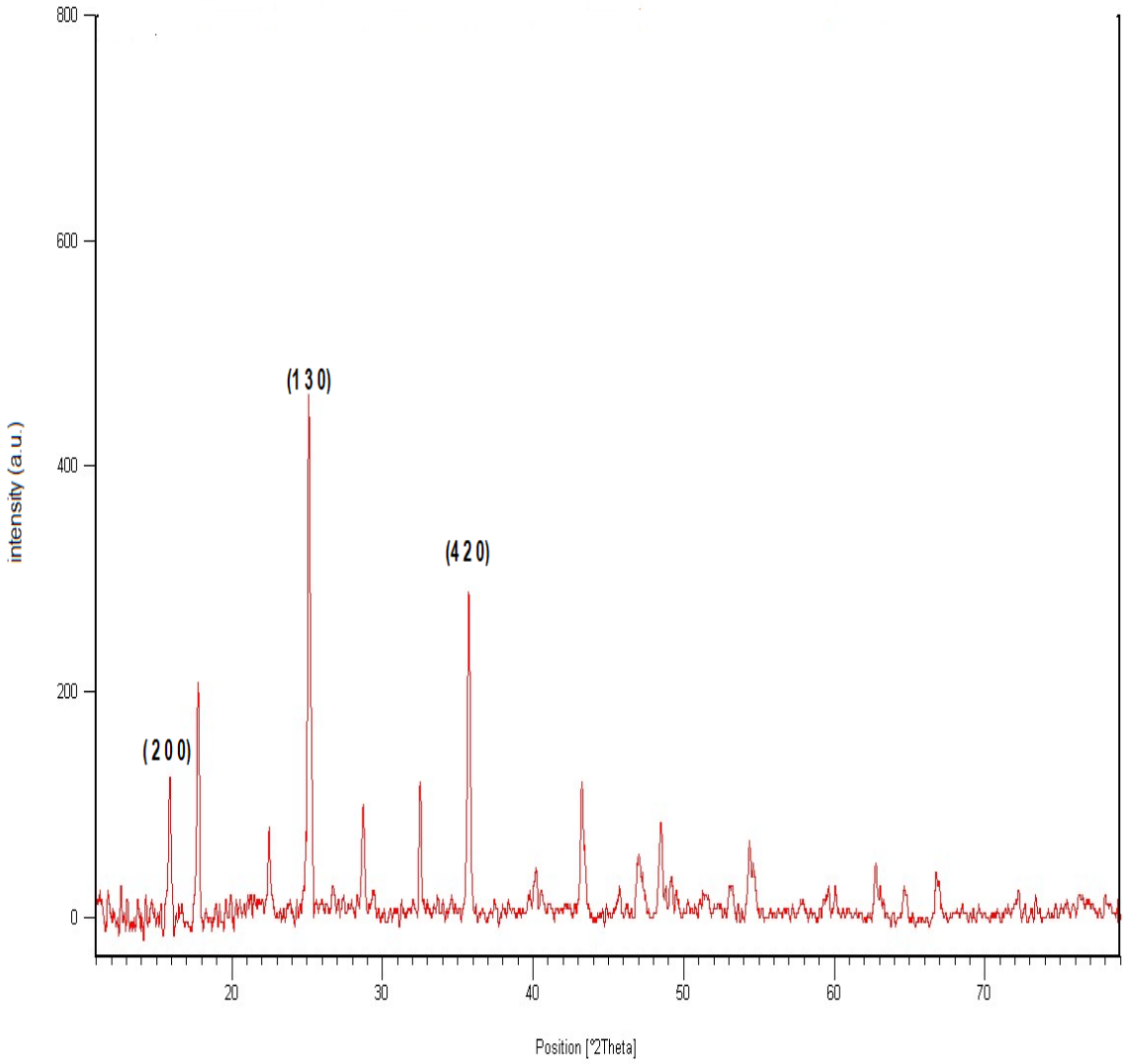

Figure 3.4: XRD pattern of 7.5% Cd doped Sb_2S_3 nanoparticles.

The above 7.5 percent Cd doped antimony sulphide nanoparticles indicated that the peaks are highly sharp which suggested that the nanoparticles are higly crystalline and as crystallinity increased nanoparticles size also increased. The average size of the nanoparticles is 34.6 nm. All the characteristic peaks were present and no extra peaks were present which indicated doping of cadmium in antimony sulphide nanoparticles.

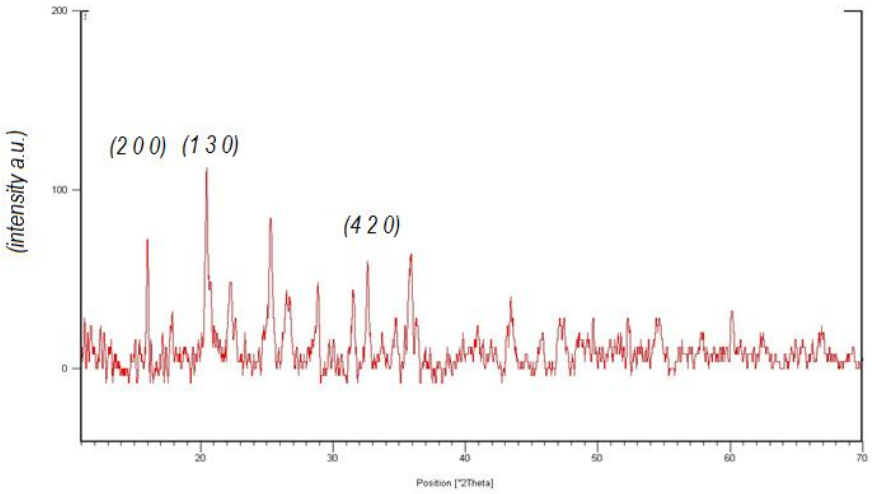

Figure 3.5: XRD pattern of 10% Cd doped Sb_2S_3 nanoparticles.

The above spectrum suggested all the characteristic sharp peaks but no extra peak was present in the spectrum for cadmium which indicated doping of cadmium in antimony sulphide nanoparticles. The average size of nanoparticles was 52.9 nm calculated by Deybe scherrer's formula.

3.2 Fourier Transform Infrared Spectroscopy (FTIR)

This is another characterization technique which was used to detect the characteristics peaks of pure antimony sulphide and doped cadmium antimony sulphide nanoparticles. The characteristics peaks of pure antimony sulphide are 335cm^{-1},274cm^{-1} and 237cm^{-1} in the FT-IR spectrum which is also clear from the spectrum of pure antimony sulphide nanoparticles [82]. The cadmium doped spectra showed that there is a clear peak shifting and disappearance of the peaks appeared which confirmed doping. The spectra are shown below.

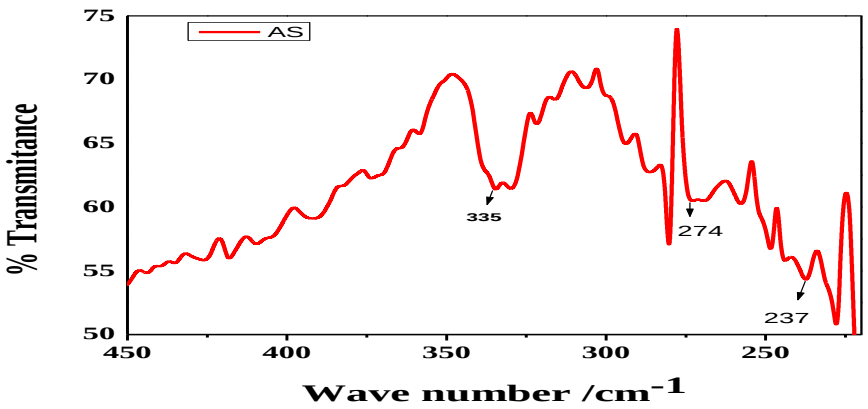

Figure 3.6: FT-IR spectrum of pure Sb_2S_3 nanoparticles.

The chararacteristic peaks of pure antimony sulphide are 335cm^{-1},274cm^{-1} and 237cm^{-1}.All these peaks are indicated by the above spectrum.

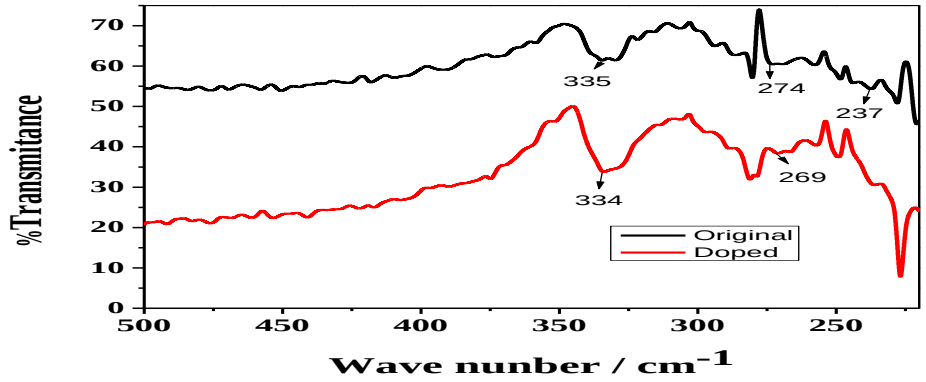

Figure 3.7: FT-IR spectrum of 2.5% Cd doped Sb_2S_3 nanoparticles

The comparison of the FT-IR spectra of pure antimony sulphide and cadmium doped antimony sulphide(2.5% cadmium doped) in the above spectrum clearly indicates the shifting in the peaks. The 335cm^{-1} peak shifts to 334cm^{-1} and 274cm^{-1} peak shifts to 269cm^{-1}.

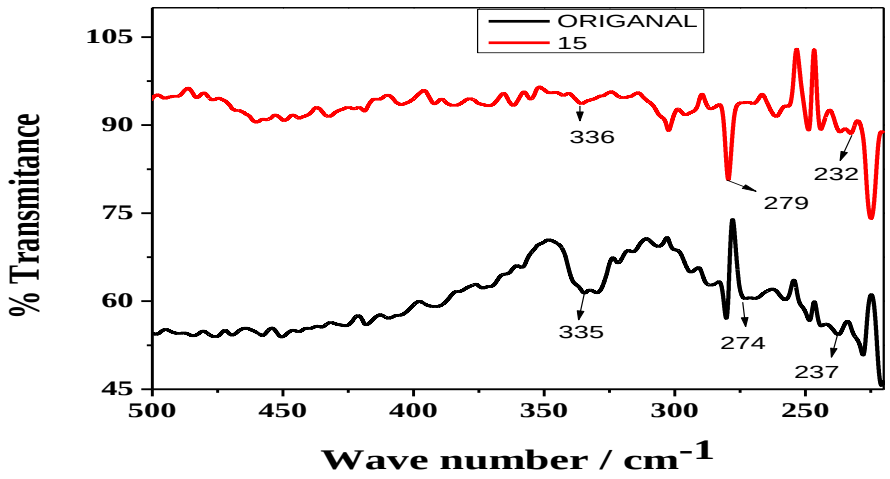

Figure 3.8: FT-IR spectrum of 5% Cd doped Sb_2S_3 nanoparticles.

The five percent cadmium doped spectrum of antimony sulphide suggested that shift has occurred in the main peaks of antimony sulphide in the above spectrum. These shifts are from 335cm^{-1} to 336cm^{-1},274cm^{-1} to 279cm^{-1} and 237cm^{-1} to 232cm^{-1}.

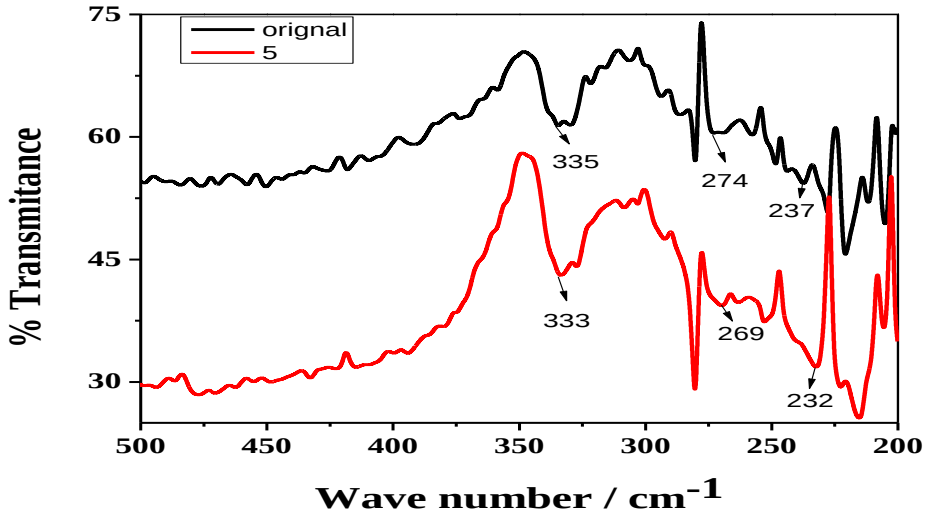

Figure 3.9: FT-IR spectrum of 7.5% Cd doped Sb_2S_3 nanoparticles.

Figure 3.9 clearly indicated that shifting in the main peaks of pure antimony occurred after doping. These shifts are from 235cm^{-1} to 333cm^{-1},274cm^{-1} to 269cm^{-1} and 237cm^{-1} to 232cm^{-1}.

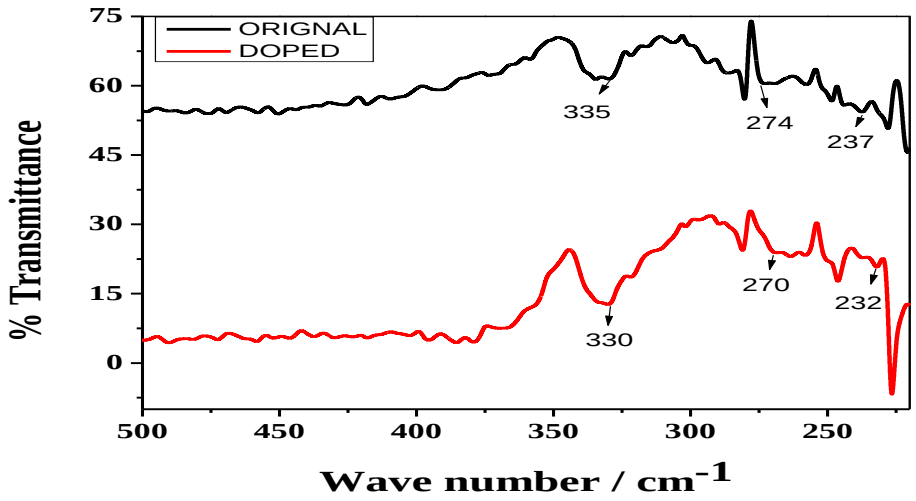

Figure 3.10: FT-IR spectrum of 10% Cd doped Sb_2S_3 nanoparticles.

The above 10 percent cadmium doped antimony sulphide also showed a clear peaks shifting in the above spectrum. These shifts are 335cm^{-1} to 330cm^{-1},274cm^{-1} to 270cm^{-1} and 237cm^{-1} to 232cm^{-1}.

3.3 Thermogravimetric Analysis (TGA)

Thermogravimetric analysis or thermal gravimetric analysis (TGA) is a method of thermal analysis in which changes in physical and chemical properties of materials are measured as a function of increasing temperature (with constant heating rate), or as a function of time (with constant temperature and/or constant mass loss)[83].

Thermo Gravimetric analysis is carried out to show the stability and thermal decomposition of organic moieties and impurities present in these nanoparticles and its dopants. Thermogravimetric analysis of these nanoparticles was done between 50 ^{0}C to 700 ^{0}C. At this range of temperature the organic impurities and other moieties have been removed and pure nanoparticles are obtained. Above 625^{0}C these nanoparticles are stable and no change is observed in weight lost which showed that these nanoparticles are highly stable and can be used at high temperature for solar cell applications. The following spectra show the stability of these nanoparticles.

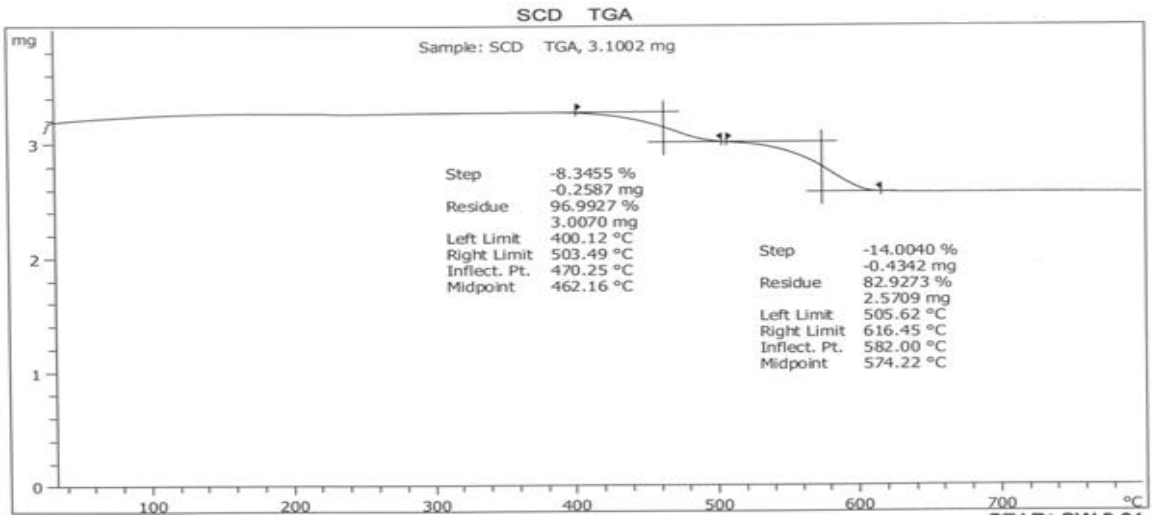

Figure 3.11: TGA of pure Sb_2S_3 nanoparticles

Figure 3.11 shows the thermogravimetric analysis (TGA) decomposition profile of the pure antimony sulphide nanoparticles under a N_2 atmosphere. The decomposition occurred in a two stages, with the onset decomposition temperature starting at ~400 °C to 503 ^{0}C and 505 ^{0}C to 616 ^{0}C. The observed residual mass (85 %) for the pure antimony sulphide and decomposed mass were (15%) showed that organic moieties and other impuritie were the major decomposition products. Based on the TGA data, the optimal decomposition temperature for the pure antimony sulphide was chosen as 500°C.

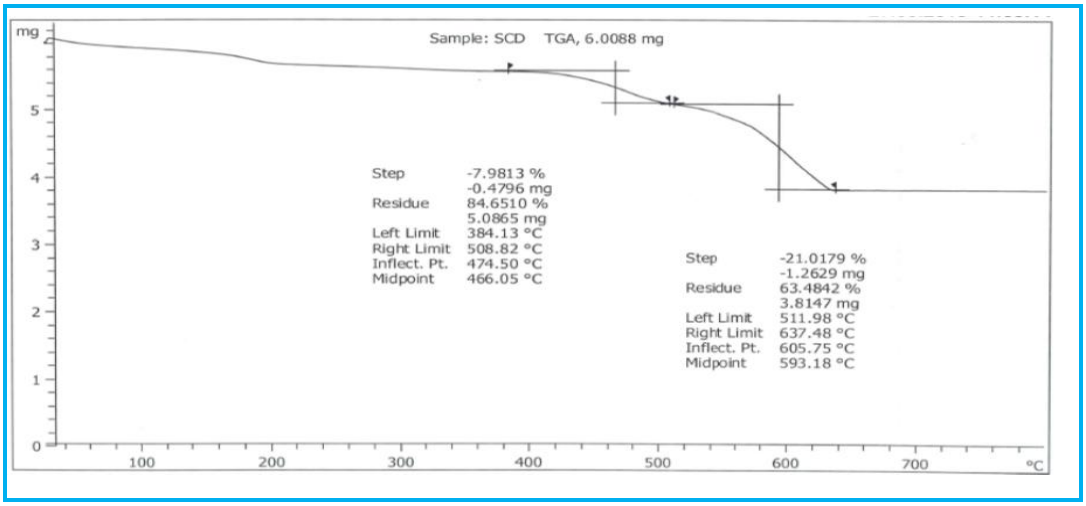

Figure 3.12: TGA of 2.5% Cd doped Sb_2S_3 nanoparticles.

Figure 3.12 cadmium doped antimony sulphide nanoparticles clearly indicated that organic moieties and impurities are decomposed in two stages between temperature ranges 384 ^{0}C to 508 ^{0}C and 511 ^{0}C to 637 ^{0}C.The amount of antimony sulphide nanoparticles residue left were (64%) and the decomposed amount were (36%).These pure Cd doped antimony sulphide were then characterized by other instrumental techniques.

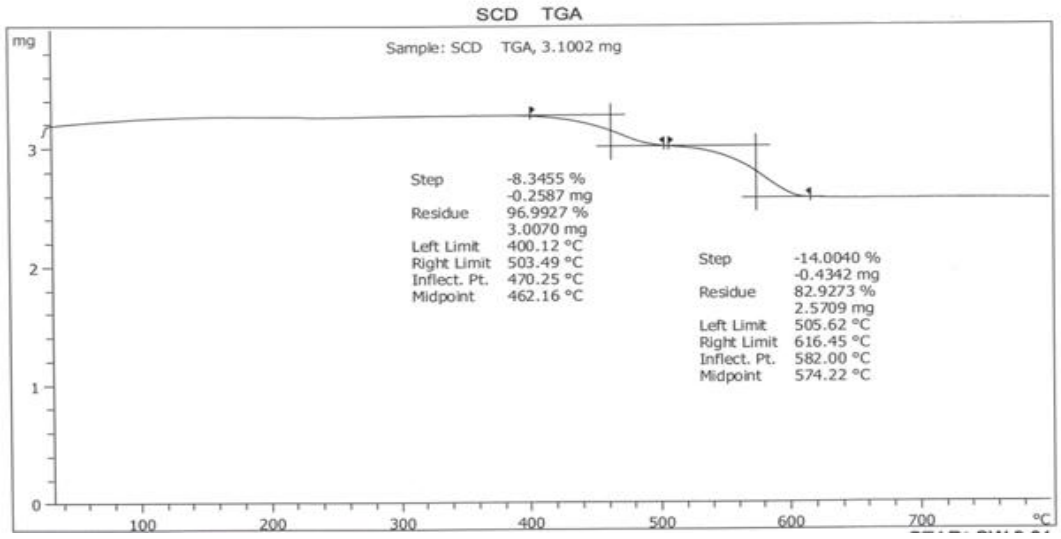

Figure 3.13: TGA of 5% Cd doped Sb_2S_3 nanoparticles.

Similarly the Thermogravimetric analysis (TGA) of 5% Cd doped antimony sulphide nanoparticles were carried out. Which indicated that organic moieties and impurities are decomposed between 400 ^{0}C to 503 ^{0}C and 505 ^{0}C to 616 ^{0}C.The amount of the sample decomposed were (17%) and the residue left were (83%).These pure Cd

doped antimony sulphide nanoparticles were then characterized by other instrumental techniques.

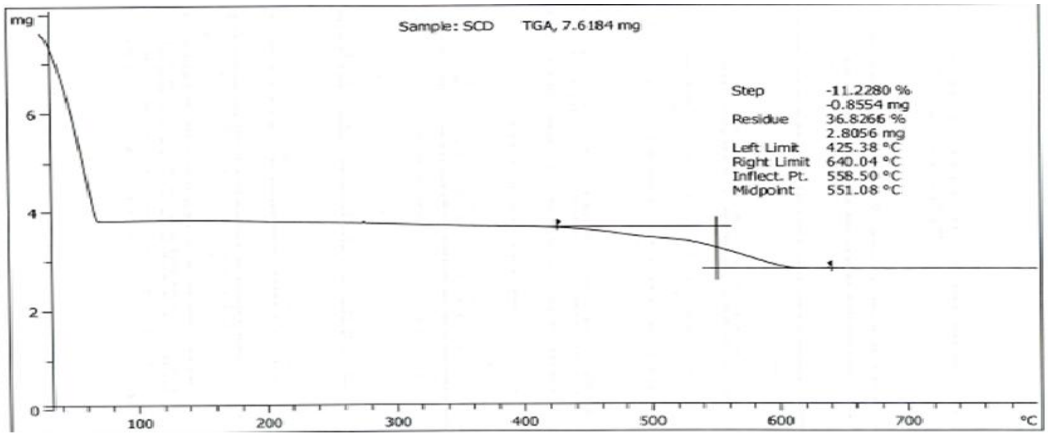

Figure 3.14: TGA of 7.5% Cd doped Sb_2S_3nanoparticles.

The spectrum of 7.5 percent Cd doped antimony sulphide indicated that these nanoparticles are highly stable.The organic moieties and impurity are decomposed between 425 ^{0}C to 640 ^{0}C.The amount left of the residue were (37%) and the rest of the decomposed amount were (63%) and the pure cadmium doped antimony sulphide nanoparticles were isolated.

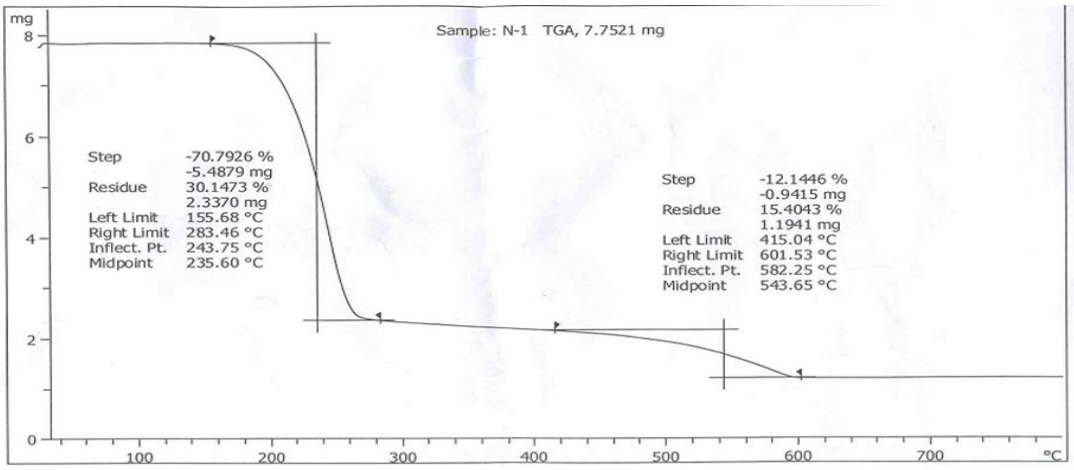

Figure 3.15: TGA of 10% Cd doped Sb_2S_3

The above spectrum showed that high decomposition of organic moieties and impurity occurred in first step and in the second step. The amount of the residue left were (16%) and the rest of the amount were decomposed (84%). The temperature range for first step decomposition were 155 ^{0}C to 283 ^{0}C and for second step it was 415 ^{0}C to 601 ^{0}C.So based on the TGA data the optimal decomposition temperature range is 500 ^{0}C for

cadmium doped antimony sulphide nanoparticles. These pure nanoparticles were characterized by other instrumental techniques.

3.4 UV-Visible Spectroscopy

Antimony sulphide and its dopants were also characterized by UV-Visible spectroscopy. UV-Visible characterization was done in ethanol. These nanoparticles and its dopants showed a clear red shift. The energy band of these nanoparticle decreases as the concentration of these dopants increases. There is a blue shift in a spectrum which is due to stiochiometric inequalities. Therefore this ratio should be in stiochiometrically equal. The wavelength of pure antimony sulphide nanoparticles were 257nm and doped nanoparticles were 268nm, 231nm, 278nm and 286nm respectively. The optical band gap of Sb_2S_3 nanoparticles was calculated from the below UV-Visible spectrum by using following formula.

$$E_g=hc/\lambda_{max}$$

Where E_g the optical band gap of the nanoparticles and λ_{max} the wavelength where maximum absorption of Sb_2S_3 occures. The calculated band gap is 3.7 eV.This value of optical band gap is corresponds to the literature value [84].

The figure below showed the uv-visible spectra of these nanoparticles.

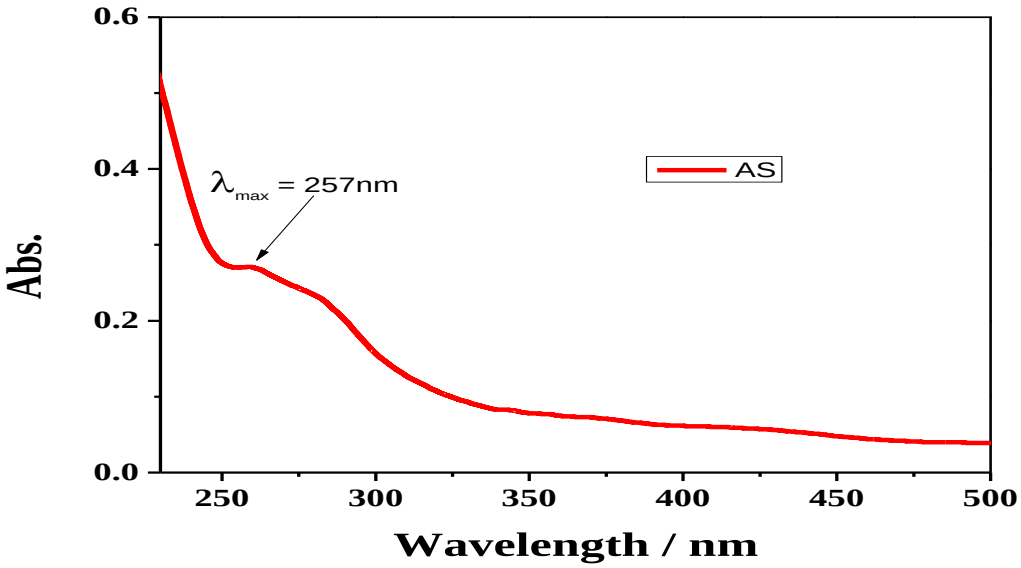

Figure 3.16: UV-Visible spectrum of pure Sb_2S_3 nanoparticles

The UV-Visible spectrum of pure antimony sulphide nanoparticles clearly showed a band at 257nm wavelength in the above figure which is reported in the literature [2].

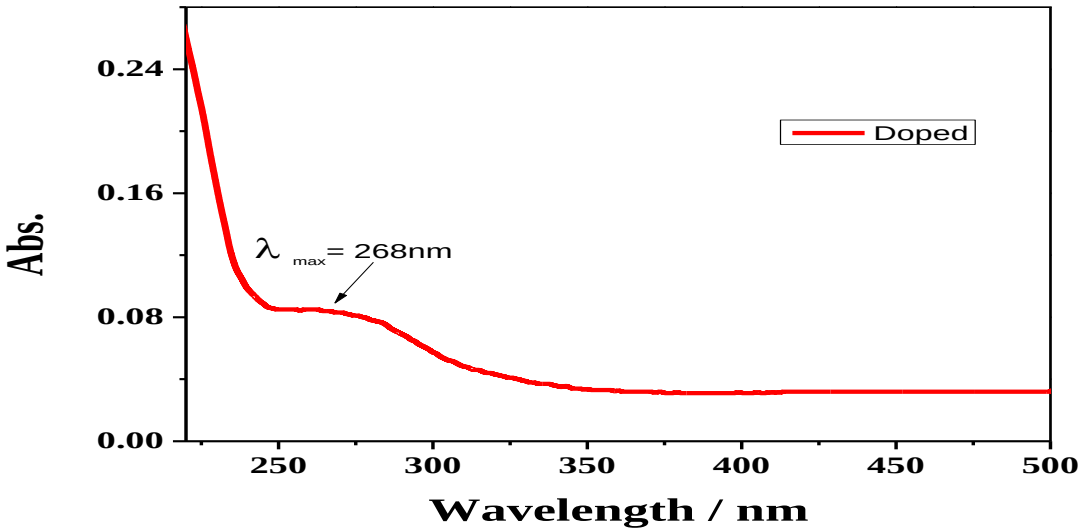

Figure 3.17: UV-Visible spectrum of 2.5% Cd doped Sb_2S_3 nanoparticles.

The UV-Visible spectrum of 2.5 percent cadmium doped antimony sulphide indicated a clear red shift in the spectrum. The wavelength range increases from 257nm to 268nm which suggested the doping of cadmium in antimony sulphide nanoparticles. This showed that as the energy band gap decreases with doping of cadmium in antimony sulphide.

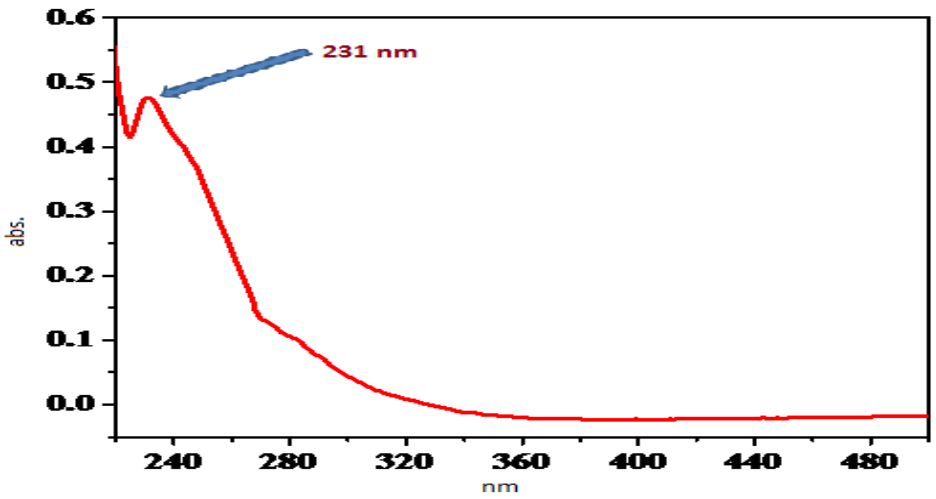

Figure 3.18: UV-Visible spectrum of 5% Cd doped Sb_2S_3 nanoparticles.

Figure 3.18 showed that red shift occurred with doping of 5 percent doping cadmium in pure antimony sulphide nanoparticles.This sometimes happens due to stiochiometric inequelities of the reacting species.The band showed at 231nm and energy band gap increases of the semiconductor materials.

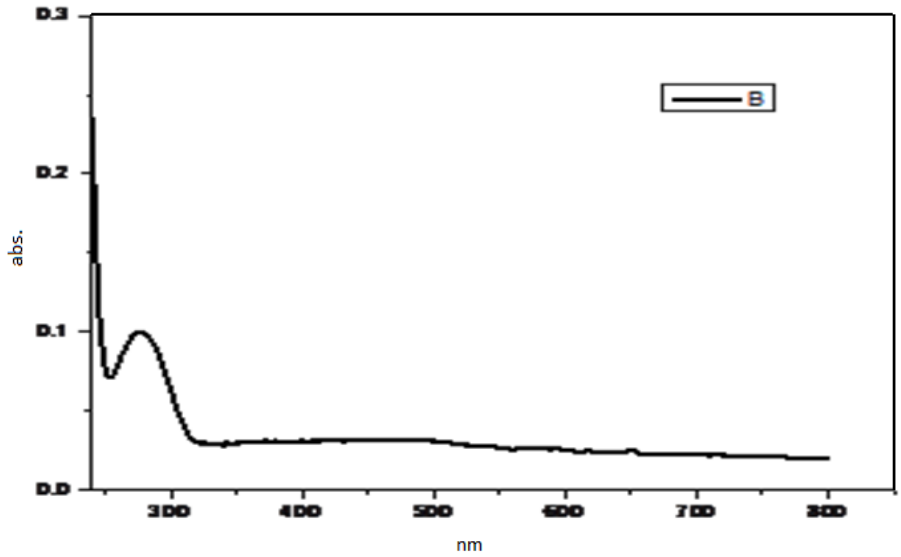

Figure 3.19: UV-Visible spectrum of 7.5% Cd doped Sb_2S_3 nanoparticles.

The UV-Visible spectrum of the 7.5 percent cadmium doped antimony sulphide clearly showed a red shift at 278nm wavelength. The energy band gap in this case again decreases Which showed that doping with cadmium increase the efficiency of semiconductor materials.

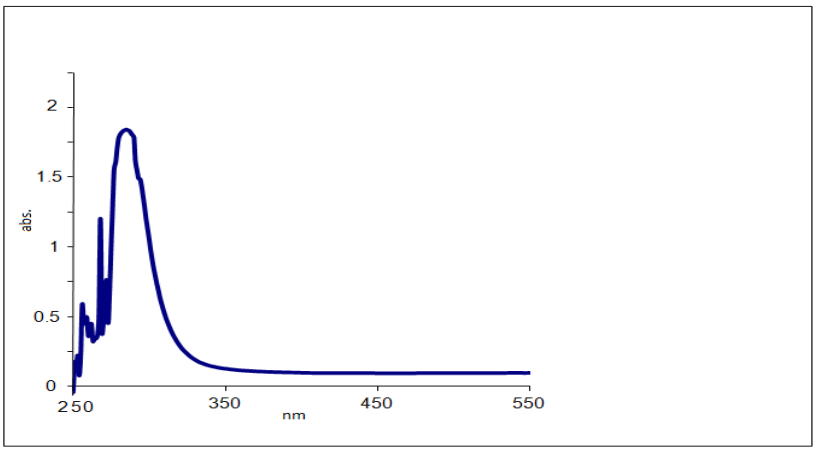

Figure 3.20: UV-visible spectrum of 10% of Cd doped Sb_2S_3 nanoparticles.

The figure above showed that as the amount of cadmium increases in the antimony sulphide nanoparticles the Fermi level decreases. The band appeared in the above figure at 286nm. This red shift is clearly indicated from the spectrum of 10 percent Cd doped antimony sulphide nanoparticles.

3.5 Scanning Electron Microscopy (SEM)

Scanning Electron Microscopy analysis was carried out to check morphology, surface topography and composition of these nanoparticles. Pure antimony sulphide nanoparticles have different morphology and surface topography from that of doped nanoparticles which shows that the particles are monodispersed, rod-like nanoparticles and the morphology is changing with increasing concentration of dopants. The dominant morphology of these nanoparticles is rod-like particles. Figures below showed the images of pure and doped nanoparticles.

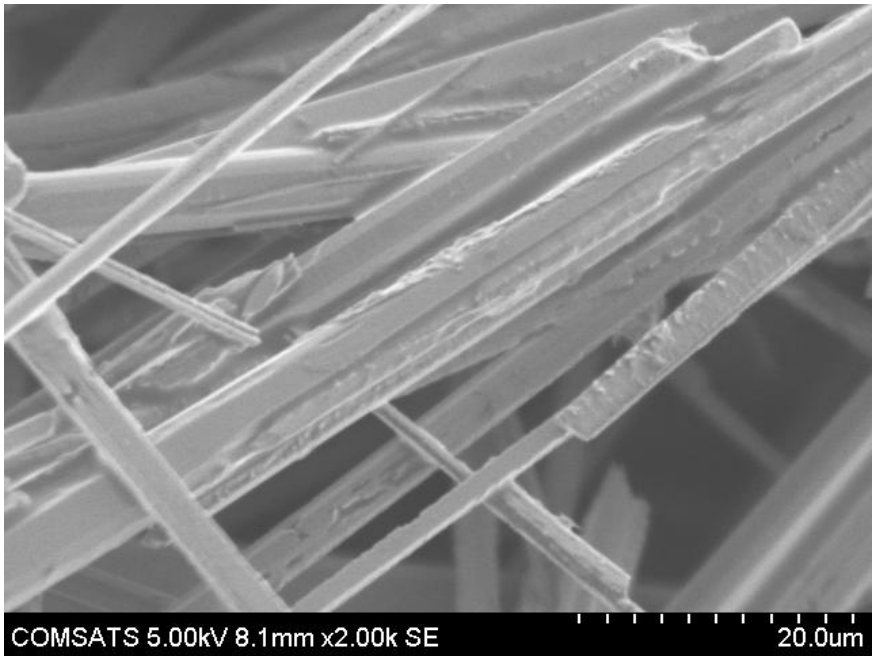

Figure 3.21: SEM spectra of pure antimony sulphide nanoparticles

Figure 3.21 shows that the nanoparticles are monodispersed and their morphology are rod-like nanoparticles. It also shows that some agglomeration of the nanoparticles indicated. These nanoparticles are large and the approximate size is 50 nm to 250 nm and well dispersed.

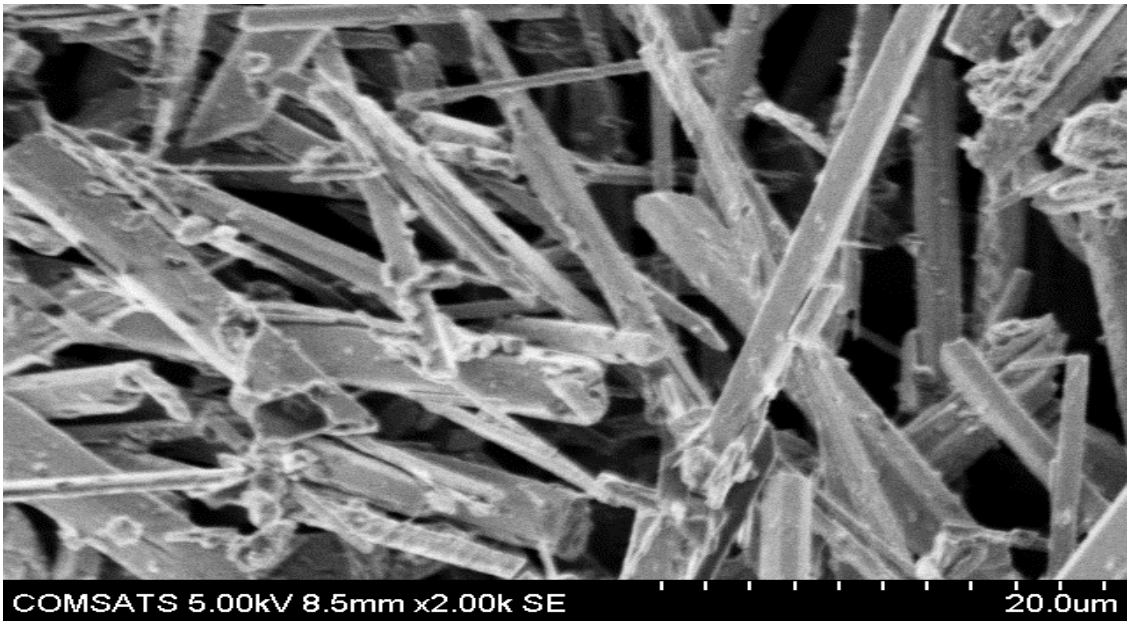

Figure 3.22: SEM spectra of 2.5% Cd doped Sb_2S_3 nanoparticles

Figure 2.5 percent doped cadmium sulphide nanoparticles indicated that the nanoparticles are homogeneously distributed. These nanoparticles have rod-like nanocrystalline structure. After doping Cd the ends of the nanoparticles are truncated and size of the nanoparticles decreased.

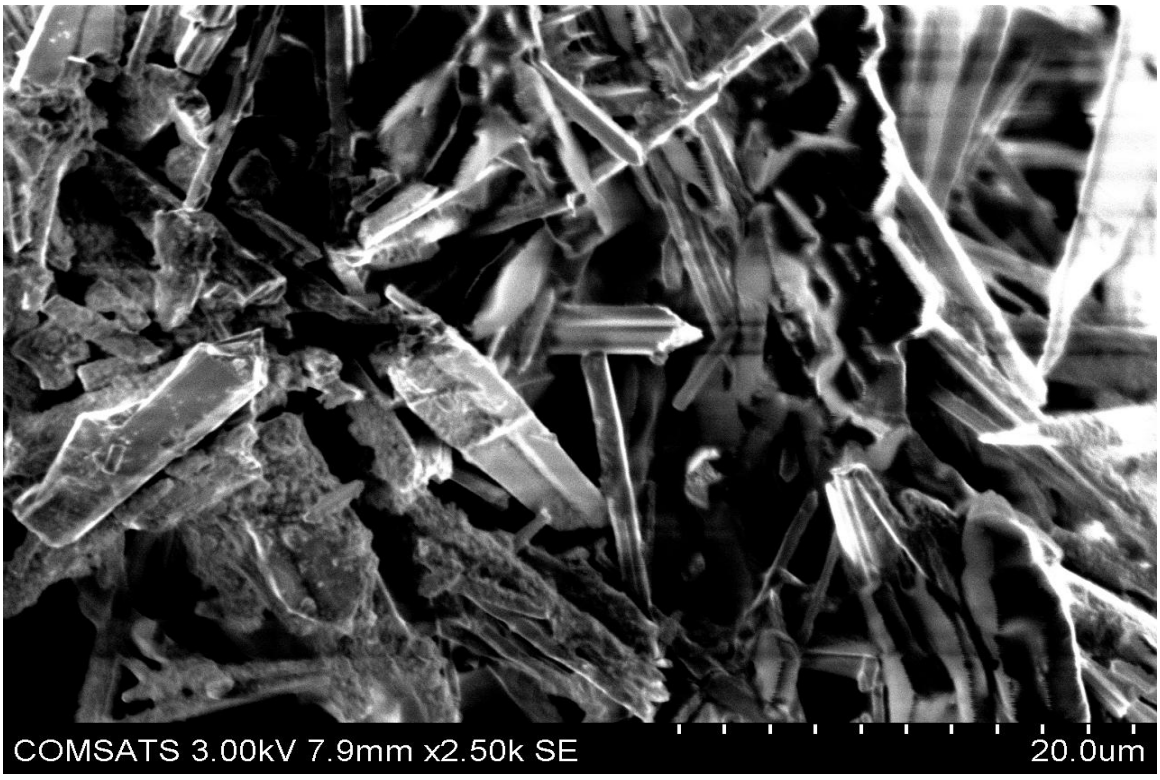

Figure 3.23: SEM image of 5% Cd doped Sb_2S_3 nanoparticles

The figure 3.23 indicated that as the concentration of cadium increases the ends of the nanoparticles are truncated and some agglomeration of nanoparticles was also observed. These nanoparticles have rod-like and flakes like morphology.

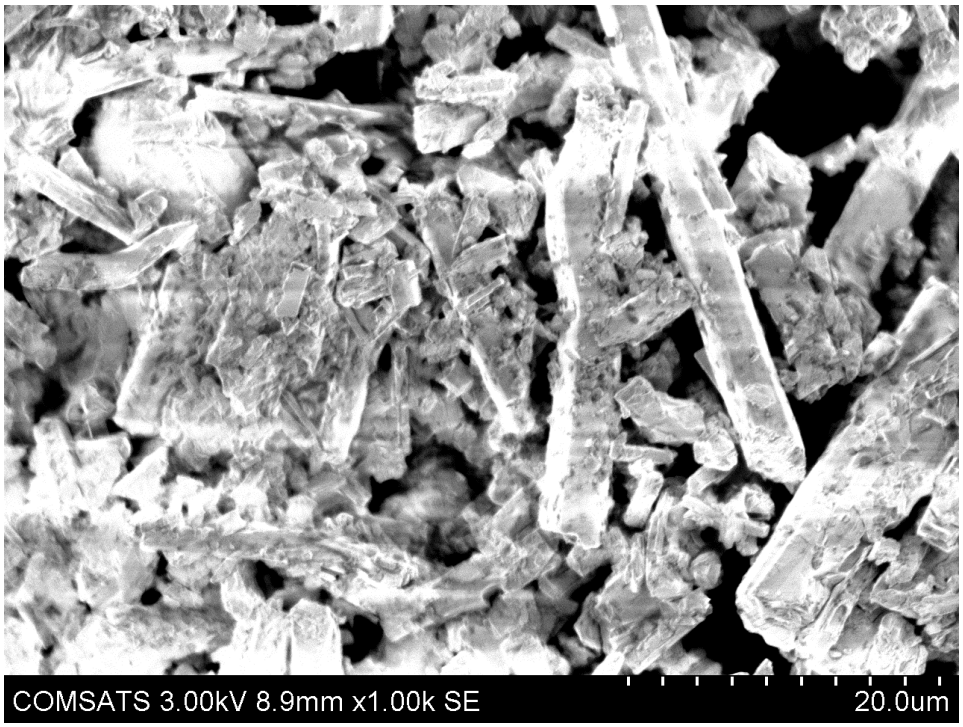

Figure 3.24: SEM Image 7.5% Cd doped Sb_2S_3 nanoparticles

The size of the nanoparticles shortened more when the concentration of cadmium is increased to 7.5 percent. There is increase in agglomeration of the nanoparticles which is indicated by SEM image.

Figure 3.25: SEM image of 10% Cd doped Sb_2S_3 nanoparticles.

Figure 3.25 indicated that the nanoparticles are agglomerated and the nanoparticles are again truncated at ends as the concentration of cadmium increases. These nanoparticles have rod-like morphology and the surface topography is rough.

3.6 Energy Dispersive Spectroscopy (EDS).

Energy Dispersive Spectroscopy (EDS) analytical technique was used to find the percentage composition of elements in the sample. The synthesized compounds containing pure antimony sulphide and cadmium doped antimony sulphide of different percent ratio were analyzed by energy dispersive spectroscopy. The analysis confirmed the doping of cadmium in antimony sulphide nanoparticles. The percentage composition of antimony, sulphur and cadmium in the synthesized sample were determined by the EDX. The EDX spectra are shown below.

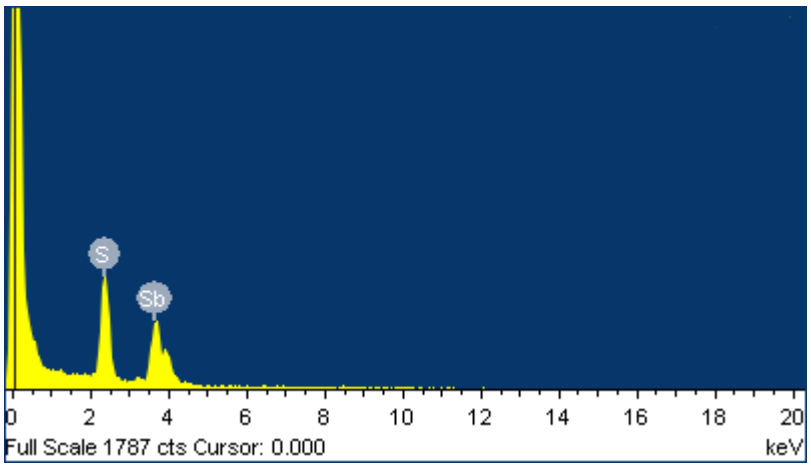

Figure 3.26: EDX spectrum of pure Sb_2S_3 nanoparticles

Figure 2.26 indicated EDX spectrum for the pure Sb_2S_3 nanoparticles were collected in order to quantify the amount of each element present in the sample.It showed that the Sb_2S_3 nanoparticles are composed of 62.3% Sulphur, 37.7% antimony atoms. These results reflect the intended antimony sulphide nanoparticles structure with more Sulphur than antimony atoms.

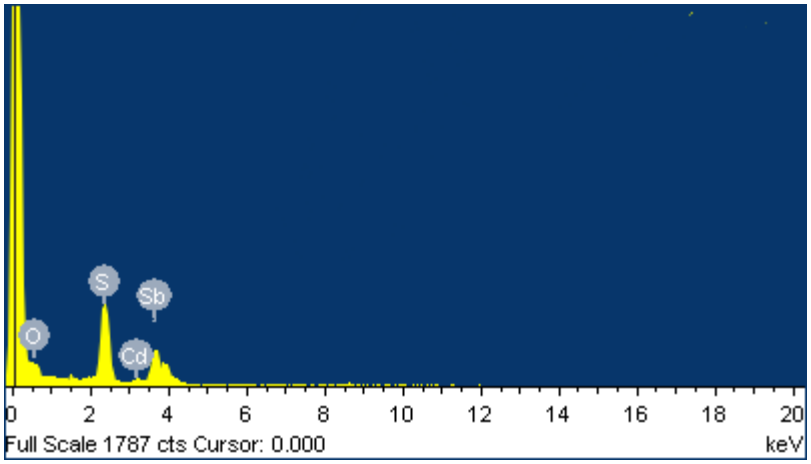

Figure 2.27: EDX spectrum of 2.5% Cd doped Sb_2S_3 nanoparticles.

Figures 2.27 show the EDX spectrums for the cadmium doped antimony sulphide nanoparticles. Here, the peaks at 2.3 keV clearly show the existence of the cadmium. The elemental analysis in EDX measurements is thought to be only for qualitative analysis. However, this spectrum of cadmium doped antimony sulphide was calculated to contain around 2.5 % cadmium relative to antimony sulphide. This finding is in accord with doped concentration of cadmium. Further, others Cd doped antimony sulphide grown exhibited this peak.

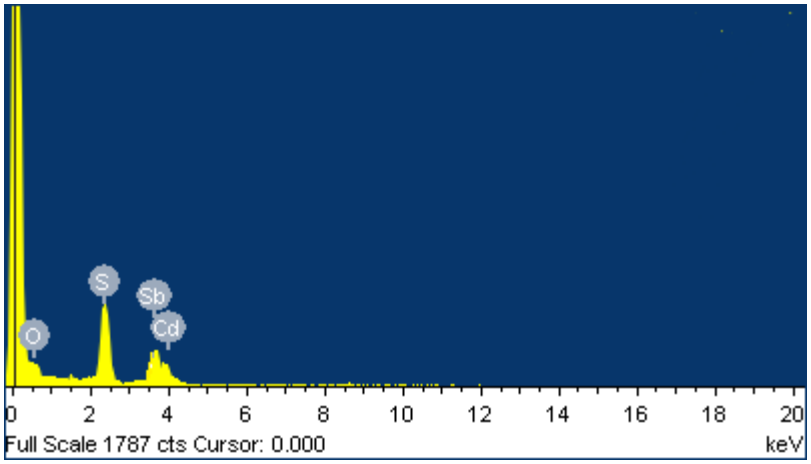

Figure 2.28: EDX spectrum of 5% Cd doped Sb_2S_3 nanoparticles.

Fig. 2.28 showed the typical EDX pattern of the sample prepared at 220 °C for 12 hours. Besides the peaks of Sb and S, there is also peak for cadmium. Values of the EDX peaks given to the atomic ratio of Sb:S were 2:3. The atomic ratio of cadmium was found

to 5%. This spectrum also indicates that the concentration of doped cadmium is increased in synthesized nanoparticles.

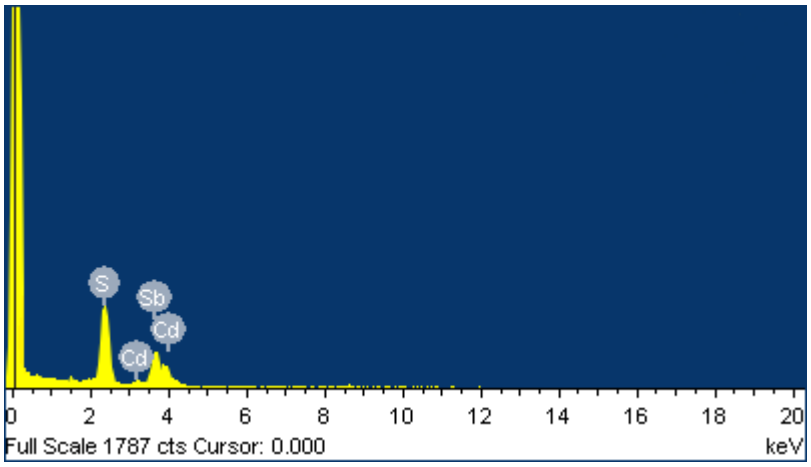

Figure 2.29: EDX spectrum of 7.5% Cd doped Sb_2S_3 nanoparticles

A further increase in concentration of cadmium was indicated by spectrum. As shown, the EDX of cadmium doped antimony sulphide confirms the presence of elements Sb,S and Cd in the product, and the obtained atomic ratio of Sb/S is well consistent with the theoretical atomic ratio (2:3). EDX spectra of cadmium doped antimony sulphide nanoparticles corresponding the products, and the atomic ratios of Sb/S/Cd basically agree with the theoretically atomic ratios.

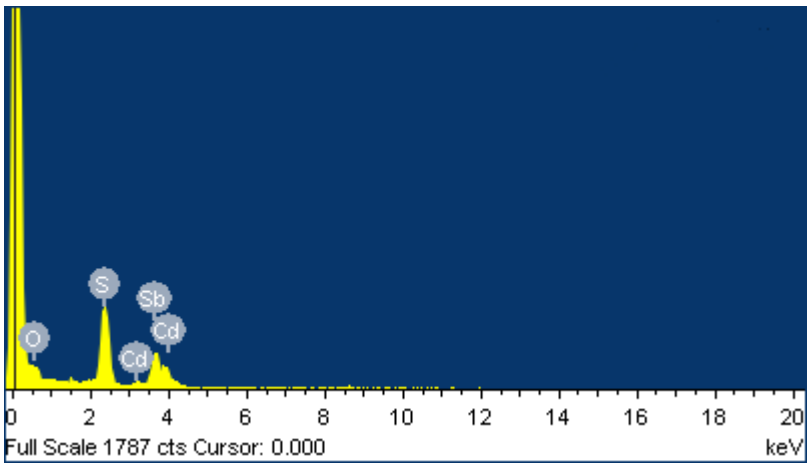

Figure 2.30: EDX spectrum of 10% Cd doped Sb_2S_3 nanoparticles.

An increase in concentration of cadmium was observed and it also indicates sulphur enrichment in the particles. The atomic ratio suggested for Sb/S/Cd was

consistent with the theoretical value. So it is clear form the above Cd doped antimony sulphide nanoparticles EDX spectrum that as the doping concentration of cadmium increased that atomic ratio of cadmium also increased.

CONCLUSION

Sb_2S_3 and Cd, Zn and Hg doped Sb_2S_3 were successfully synthesized by using hydrothermal method in autoclave. The synthesized catalysts were characterized by powder XRD, UV-Vis & FT-IR spectroscopy, TGA and SEM. Powder XRD analysis showed excellent crystalline nature of the synthesized catalysts having crystallite size less then 35 nm. From UV-Visible data, band gap obtained was 3.5 eV to 3.7 eV where as Sb_2S_3 in bulk have band gap of 1.88 eV. The λ_{max} obtained for Sb_2S_3 was 257 nm however with the increasing percent of dopant causes and red shift, confirming the doping. The shifts in wave number (cm^{-1}) value also justifying the doping of Cd, Zn and Hg atoms in Sb_2S_3 nanocrystalline structures. The thermal gravimetric curves show the high stability of synthesized catalysts. The morphology and uniform dispersion of dopant is revealed by SEM analysis. The EDX confirmed doing of the cadmium in the antimony sulphide nanoparticles and also showed the percentage composition of the elements.

REFERENCES

1. "National Institute of Environmental Health Sciences USA". www.niehs.nih.gov/health/topics/agents/sya-nano
2. "World Energy, Technology and Climate policy Outlook". [http://ec.europa.eu/research/energy/gp/gp_pu/article_1257_en.htm].
3. J. A. Collins, "An Update on Progress in the Development of Electrocatalyst Materials for Direct Methanol Fuel Cells", Energy Marie Courie Fellowship Conference, 10-14 Oct (2001) online.
4. www.fuel cells.org
5. B. J. Holland, J. G. Zhu, L. Jamet," fuel cells technology and applications".
6. G. Hoogers, Fuel Cells Technology Handbook, Boca Raton, FL, CRC PRESS, 2003.
7. V. M. Anischik, V. E. Borisenko, S. A. Zhdanok, N. K. Tolochko, V. M. Fedosyuk Nanomaterials and Nanotechnologies. Minsk: Izd. BGU. [The review of various kinds of nanomaterials and nanotechnology] [In Russian] 2008.
8. V. E. Borisenko, N. K. Tolochko**.** Nanotechnologies: Stages of Development. nauka i innovatsii (Minsk), No. 12, 66-68. [The basic stages of nanotechnology development are considered] [In Russian] 2008.
9. L. Foster, Nanotechnology Science, Innovation and Opportunity. Prentice Hall, New York. [The review of condition and development prospects of nanotechnology, and also possible influences of nanotechnology on global processes] 2005.
10. C. J. Poole, F. Owens, Introduction to Nanotechnology, Wiley, [The review of structure and properties, manufacturing techniques, methods of research and areas of application of nanomaterials] 2003.
11. N. G. Dhere, Solar Energy Materials & Solar Cells, 91, 137, 2007.
12. United Nations Development Programme, World Energy Assessment, Energy and the challenge of Sustainability, UNDP, New York, ISBN 92-1-1261-0 (Chapter 5: Energy Resources).
13. Massachusetts Institute of Technology, The Future of Coal, Options for a Carbon Constrained World (MIT, Cambridge, MA, 2005).

14. Energy Information Administration, U.S. Department of Energy, World Net Nuclear Electric Power Generation, 1980-2005, (EIA, U.S. Department of Energy, Washington DC. 2007)
15. The Intergovernmental Panel on Climate Change, IPCC Fourth Assessment Report (AR4) (IPCC, 2007).
16. R. E. H. Sims, M.R.S. Bulletin, 33, 389, 2008.
17. http://gcep.stanford.edu/pdfs/QeJ5maLQQrugiSYMF3ATDA/2.2.6.green_06.pdf
18. "Publications, Presentations, and News Database: Cadmium Telluride". National Renewable Energy Laboratory.
19. K. Zweibel, J. Mason, V. Fthenakis, "A Solar Grand Plan", Scientific American, Jan 2008. CdTe PV is the cheapest example of PV technologies and prices are about 16¢/kWh with US Southwest sunlight.
20. H. Wan, "Dye Sensitized Solar Cells", University of Alabama Department of Chemistry, p. 3.
21. Milliron, J. Delia, Gur, Ilan; Alivisatos, A. Paul (2005). "Hybrid Organic–Nanocrystal Solar Cells". M.R.S. Bulletin 30: 41–44. doi:10.1557/mrs2005.8
22. W. Heywang, K. H. Zaininger, Silicon: the semiconductor material, in Silicon: evolution and future of a technology, P. Siffert, E. F. Krimmel eds., Springer Verlag, 2004.
23. H. Alexander, Thon, M. Susanna M, Hoogland, Sjoerd, Voznyy, Oleksandr, Zhitomirsky, David, Debnath, Ratan, Levina, Larissa, Rollny, R. Lisa R, Carey, H. Graham, Fischer, Armin; Kemp, W. Kyle, Kramer, J. Illan, Ning, Zhijun, Labelle, André J, Chou, Kang Wei, Amassian, Aram, Sargent, H. Edward**.** **(**2012). "Hybrid passivated colloidal quantum dot solids". Nature Nanotechnology **7**: 577–582. doi:10.1038/nnano.2012.127
24. Renewable Energy Magazine.
25. P. Reiss, Synthesis of semiconductor nanocrystals in organic solvents, A.L. Rogach, (ed.) Semiconductor Nanocrystal Quantum Dots, Synthesis Assembly, Spectroscopy, and Applications. Springer-Verlag; Vienna (Austria),35–72,2008.
26. Q. Guo, S. J. Kim, M. Kar, W. N. Shafarman, R. W. Birkmire, E. A. Stach, Nano Lett., 8, 2982, 2008.
27. A. J. Nozik, Chem. Phys. Lett., 457, 3, 2008.
28. M. C. Beard, R. J. Ellingson. Laser Photonics Rev., 2, 377, 2008.

29. J. A. McGuire, J. Joo, J. M. Pietryga, R. D. Schaller, V. I. Klimov, Acc. Chem. Res., 41, 1810, 2008.
30. H. W. Hilhouse, M. C. Beard, Current Opinion in Colloid & Interface Sci., 14, 245, 2009.
31. N. G. Dhere, Solar Energy Materials & Solar Cells, 91, 1376, 2007.
32. United Nations Development Programme, World Energy Assessment, Energy and the challenge of Sustainability, UNDP, New York, ISBN 92-1-1261-0 (Chapter 5: Energy Resources)
33. D. M. Chapins, C. S. Fuller and G. L. Pearson, J. Appl. Phys., 25, 676, 1954.
34. European Commission, A Vision for Photovoltaic Technology, Report by the Photovaltaic Technology Advisory Research Council (PV-TRAC), European Commission, Brussels, Belgium, 2005.
35. V. Fthenakis, Renewable and Sustainable Energy Reviews, 13, 2746, 2009.
36. J. Zhao, A. Wang, M. A. Green and F. Ferraza, Appl. Phys. Lett., 73, 1991, 1998.
37. D. L. King, W. K. Shubert and T. D. Hund, Conference Record, 1st World Conference on Solar Energy Conversion, Hawaii, 1660, 1994.
38. D. M. Bagnall and M. Boreland, Energy Policy, 36, 4390, 2008.
39. L. Kazmerski, Renewable and Sustainable Energy Reviws, 1, 71, 1997.
40. K. Zweibel and M. A. Green, Millenium Issue, Prog. Photovaltaics, 8, 1, 2000.
41. J. Meier, J. Sitznagel, U. Kroll, C. Bucher, S. Fay, T. Moriarty and A. Shah, Thin Solid Films, 451, 518, 2004.
42. J. Yang, A. Banerjee, T. Glatfelter, K. Hoffman, X. Xu and S. Guha, Conference Records, 1st World Conference on Photovolatic Energy Conversion, Hawaii, 380, December 1994.
43. K. Yamamoto, M. Yoshimi, T. Suzuki, T. Nakata, T. Sawada, A. Nakajima and K.Hayashi, Proceedings of the 28th IEEE Photovoltaic Specialists Conference-Anchorage, IEEE, New York, 1428, 2000.
44. K. L. Chopra, P. D. Paulson and V. Dutta, Prog. Photovolt. Res. Appl., 12, 69, 2004.
45. P. A. Cox, The Electronic Structure and Chemistry of Solids, 6th ed. Oxford University Press, 1995.
46. H. P. Myers, Introductory Solid State Physics, Taylor and Francis, London, 1990.
47. H. M. Rosenberg, The Solid State, Oxford University Press, 1987.

48. G. K. Cranstoun et al., J. Electronic Spectroscopy and Related Phenomena, 33(1), 23, 1984.
49. T. Trindade, P. O'Brien, X. Zhang, M. Motevalli, J. Mater. Chem., 7, 1011, 1997.
50. H. Maghraoui-Meherzi, T. Ben-Nasr, N. Kamoun, M. Dachraoui. J. Phys. B. Condense Mater., 405, 3101, 2010.
51. X. Cao, L. Gu, Z. Wang, W. Gao, L. Zhuge, Y. Li. J. Cryst. Growth, 286, 96, 2006.
52. W. Lou, M. Chen, X.Wang, W. Liu. J. Chem Mater, 19, 872, 2007.
53. G.Y. Chen, B. Dneg, G.B. Cai, T.K. Zhang, W.F. Dong. J. Phys. Chem C, 112, 672, 2008.
54. G. Y. Chen, W. X. Zhang, A.W. Xu. J. Mater Chem. Phy. 123, 236, 2010.
55. L. Chen, W. Zhu, Q. Han , X. Yang, L. Lu, X. Wang. J. Mater Lett., 63, 253, 2009.
56. X. Cao, Y. Xie, L. Li . J. Solid State Chem., 2004, 177, 202, 2009.
57. D. Wang, G. Song, X. Fu, X. Li. J. Cryst. Growth, 281, 611, 2005.
58. P. Salinas-Estevané, E. M. Sánchez. J. Cryst. Growth Des., 10, 3917, 2010.
59. P. Salinas-Estevané, E. M. Sánchez. J. Mater. Lett., 64, 2627, 2010.
60. X. Chen, X. Zhang, C. Shi, X. Li, Y. Qian. J. Solid State Commun., 134, 613, 2005.
61. B. Cheng, E. T. Samulski. J. Mater Res. Bull, 38, 297, 2003.
62. C. Li, X. Yang, Y. Liu, Z. Zhao, Y. Qian. J. Cryst. Growth, 255, 342, 2003.
63. Y. Xu, Z. Ren, G. Cao, W. Ren, K. Deng, Y. Zhang. J. Cryst. Res. Technol., 44, 851, 2009.
64. H. Yang, X. Su, A. Tang. J. Mater. Res. Bull., 42, 1357, 2007.
65. A. M. Qin, Y. P. Fang, W. X. Zhao, H. Q. Liu, C. Y. Su. J. Cryst. Growth, 283, 230, 2005.
66. M. Salavati-Niasari, M.R. Loghman-Estarki, F. Davar. J. Alloys Compd.,475, 782, 2009.
67. M. Salavati-Niasari, A. Sobhani, F. Davar. J. Alloys Compd., 507, 77, 2010.
68. M. Salavati-Niasari, D. Ghanbari, F. Davar. J. Alloys Compd., 488, 442, 2009.
69. M. Salavati-Niasari, F. Davar, M. R. Loghman-Estarki. J. Alloys Compd.,481, 776, 2009.
70. A. M. Qin, Y. P. Fang, W. X. Zhao, H. Q. Liu, C.Y. Su. J. Cryst. Growth, 283, 230, 2005.
71. M. Salavati-Niasari, M. R. Loghman-Estarki, F. Davar. J. Alloys Compd., 475,

782, 2009.

72. M. Salavati-Niasari, A. Sobhani, F. Davar. J. Alloys Compd., 507, 77, 2010.
73. M. Salavati-Niasari, D. Ghanbari, F. Davar. J. Alloys Compd., 488, 442, 2009.
74. M. Salavati-Niasari, F. Davar, M. R. Loghman-Estarki. J. Alloys Compd., 481, 776, 2009.
75. D. Wang, G. Song, X. Fu, X. Li. J. Cryst. Growth, 281, 611, 2005
76. L. Chen, W. Zhu, Q. Han, X. Yang, L. Lu, X. Wang. J. Mater. Lett., 63, 253, 2009.
77. C. Q. Nguyen, A. Adeogun, M. Afzaal, M. A. Malik and P. O'Brien, Chem. Commun., 2179, 2006.
78. C.Q. Nguyan, A. Adeogun, M. Afzaal and P.O'Brien,Chem.Commun., 2182, 2006.
79. X. Wu, J. C. Keane, R. G. Dhere, C. DeHart, A. Duda, T. A. Gessert, S. Asher,D.H. Levi and P. Sheldon, Proceedings of 17th European Photovoltaic Solar Energy Conference, Munich, 995, 2001.
80. X. Chen, X. Zhang, C. Shi, X. Li, Y. Qian. J. Solid State Commun., 134, 613, 2005.
81. Y. Xu, Z. Ren, G. Cao, W. Ren, K. Deng, Y. Zhang. J. Cryst. Res. Technol., 44, 851, 2009.
82. A. L. Fahrenbruch and R. H. Bube. in "Fundamentals of Sollar Cells", Photovoltaic Solar Energy Conversion, Academic Press, New York, 1983.
83. P. Niedzielski, M. Siepak. Analytical methods for determining arsenic, Antimony and Selenium in environmental samples. Pol. J. Environ. Stud., 12, 653, 2003.
84. A. W. Coats and J. P. Redfern. "Thermogravimetric Analysis, A Review", Analyst 88, 906, 1963.